

Thermal evolution and physics of melt extraction on the ureilite parent body

Lionel Wilson^{a,*}, Cyrena Anne Goodrich^b, James A. Van Orman^c

^a *Environmental Science Department, Lancaster University, Lancaster LA1 4YQ, UK*

^b *Department of Physical Sciences, Kingsborough Community College, 2001 Oriental Blvd, Brooklyn, NY 11235, USA*

^c *Department of Geological Sciences, Case Western Reserve University, Cleveland, OH 44120, USA*

Received 21 December 2007; accepted in revised form 19 September 2008; available online 4 October 2008

Abstract

We develop a physical model of the thermal history of the ureilite parent body (UPB) that numerically tracks the history of its heating, hydration, dehydration, partial melting and smelting as a function of its formation time and the initial values of its composition, formation temperature and water ice content. Petrologic and chemical data from the main group (non-polymict) ureilite meteorites, which sample the interior of the UPB between depths corresponding to pressures in the range 3–10 MPa, are used to constrain the model. We find that to achieve the ~30% melting inferred for ureilites from all sampled depths, the UPB must have had a radius between ~80 and ~130 km and must have accreted about 0.55 Ma after CAI formation. Melting began in the body at ~1 Ma after CAI, and the time at which 30% melting was reached varied with depth in the asteroid but was always between ~4.5 and ~5.8 Ma after CAI. The total rate at which melt was produced in the UPB varied from more than 100 m³ s⁻¹ in the very early stages of melting at ~1 Ma after CAI to ~5 m³ s⁻¹ between 2 and 3 Ma after CAI, decreasing to extremely small values as the end of melting was approached beyond ~5 Ma. Although the initial period of high melt production occupied only a short time around 1 Ma after CAI, it corresponded to ~half (16%) of total silicate melting, and all strictly basaltic (i.e. plagioclase-saturated) melts must have been produced during this period.

A very efficient melt transport network, consisting of a hierarchy of veins and larger pathways (dikes), developed quickly at the start of melting, ensuring rapid (timescales of months) transport of any single parcel of melt to shallow levels, thus ensuring that chemical interaction between melts and the rocks through which they subsequently passed was negligible. Volatile (mainly carbon monoxide) production due to smelting began at the start of silicate melting in the shallowest parts of the UPB and at later times at greater depths. Except at the very start and very end of melting, the volatile content of the melts produced was always high – generally between 15 and 35 mass % – and most of the melt produced was erupted at the surface of the UPB with speeds well in excess of the escape velocity and was lost into space. However, we show that 30% melting at the 3 MPa pressure level was only possible if ~15% of the total melt produced in the asteroid was retained as a small number (~5) of very extensive, sill-like intrusions centered at a depth of ~7 km below the surface, near the base of the ~8 km thick outer crust of the asteroid that was maintained at temperatures below the basalt solidus by conductive heat loss to the surface. The horizontal extents of these sills occupied about 75% of the surface area of the UPB, and the sills acted as buffers between the steady supply of melt from depth and the intermittent explosive eruption of the melt into space. We infer that samples from these intrusions are preserved as the rare feldspathic (loosely basaltic) clasts in polymict ureilites, and show that the cooling histories of the sills are consistent with these clasts reaching isotopic closure at ~5 Ma after CAI, as given by ²⁶Al–²⁶Mg, ⁵³Mn–⁵³Cr and Pb–Pb age dates.

© 2008 Elsevier Ltd. All rights reserved.

* Corresponding author.

E-mail address: L.Wilson@lancaster.ac.uk (L. Wilson).

1. INTRODUCTION

Ureilites, which form the second largest group of achondrites (240 samples), are coarse-grained, highly-equilibrated ultramafic rocks that are thought by most workers to represent the residual mantle of a partially melted, carbon-rich asteroid (see reviews by Goodrich, 1992; Mittlefehldt et al., 1998; Goodrich et al., 2004). One of their distinctive characteristics is their “primitive” (i.e. chondrite-like) oxygen isotopic signature, which suggests that they preserve a unique stage of early planetary differentiation. This paper presents calculations of the heating, melting, and physics of melt extraction on the ureilite parent body (UPB) during this early period of its history, based on the petrologic and geochemical model developed in Goodrich et al. (2007). Here, we briefly summarize the background and most salient aspects of that model.

The majority of ureilites consist of olivine + low-Ca pyroxene (pigeonite and/or orthopyroxene), with interstitial carbon (graphite \pm secondary, shock-produced diamond) and metal (\pm sulfide and/or phosphide) as the only common accessory phases. Their olivine compositions (constant within each sample) show a large range of Fo (molar $\text{Mg}/[\text{Mg} + \text{Fe}]$) values ($\sim 76\text{--}92$) at essentially constant Mn/Mg, which indicates that they are related to one another principally by various degrees of oxidation or reduction rather than various degrees of melting (Mittlefehldt, 1986; Goodrich et al., 1987; Goodrich and Delaney, 2000). This redox relationship can be explained by smelting (pressure-dependent carbon redox reactions: in simplest form, $\text{FeO} + \text{C} \rightarrow \text{Fe} + \text{CO}$) over a range of pressures in the ureilite parent body (Berkley and Jones, 1982; Goodrich et al., 1987, 2007; Warren and Kallemeyn, 1992; Walker and

Grove, 1993; Sinha et al., 1997; Singletary and Grove, 2003), an interpretation that is supported by a correlation of Fo with pyroxene/olivine ratio (Singletary and Grove, 2003; Goodrich et al., 2007) and by the restriction of orthopyroxene to the few most magnesian ($\text{Fo} \geq 86$) samples (Goodrich et al., 2007). The smelting model is thus highly successful at explaining many of the petrologic and chemical features of ureilites that would be difficult to explain in a normal igneous fractionation model (particularly the large range of Fo values). It may be less successful at explaining their metal and siderophile element abundances. Smelting predicts a correlation of Fo, not only with pyroxene/olivine ratio, but also with metal content or (if the metal is removed) siderophile element abundances. In fact, ureilites have uniformly low metal contents (at most a few percent) and show no correlation of siderophile elements with Fo. Although some workers (Mittlefehldt et al., 2005; Warren and Huber, 2006; Warren et al., 2006) have argued that this observation is fatal for the smelting model, we have suggested one hypothesis that may explain it (Goodrich et al., 2007) and believe there are other possibilities as well. The present work is thus based on a smelting model, under the assumption that future work will be able to reconcile it with the metal and siderophile element abundances in ureilites.

In this model, the olivine + low-Ca pyroxene ureilites represent the mantle of a ureilite parent body (UPB) that was stratified (or had a radial gradient) in *mg* (molar $\text{Mg}/[\text{Mg} + \text{Fe}] = \text{Fo}$ in referring to olivine), pyroxene/olivine ratio, and pyroxene type (Fig. 1), due to the pressure dependence of carbon redox reactions. Ureilite smelting (i.e. final equilibration) pressures have been estimated using a variety of thermodynamic treatments and experimental methods

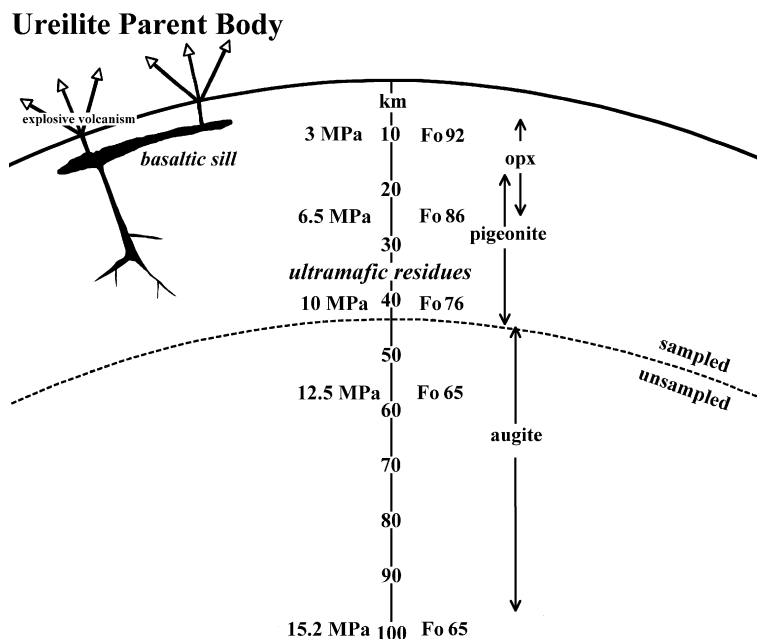


Fig. 1. Schematic cross-section of the ureilite parent body (UPB), showing relationship between depth (km), pressure (MPa), Fo (molar $\text{Mg}/[\text{Mg} + \text{Fe}]$) of olivine, and pyroxene type (opx = orthopyroxene) in the smelting model developed in Goodrich et al. (2004, 2007) and this paper. Here, we focus on the formation of shallow crustal basaltic intrusions (“a sill”).

(Berkley and Jones, 1982; Goodrich et al., 1987; Warren and Kallemeyn, 1992; Walker and Grove, 1993; Sinha et al., 1997; Singletary and Grove, 2003), with the most reliable results being ~9–10 MPa for the most ferroan ureilite and ~2–3 MPa for the most magnesian. Here, we assume that the total range of pressures sampled by the meteorites is ~3–10 MPa, as determined in Goodrich et al. (2007).

What is missing from this picture, from the point of view of planetary differentiation, is the melts. A few ureilites that are augite-bearing appear to be ultramafic cumulates rather than residues (Goodrich et al., 2004, 2006), but the fact that they have Fo values in the same range as the olivine + low-Ca pyroxene ureilites suggests that they formed over the same range of depths. There are no basaltic ureilites, and thus the only direct petrologic information we have about the melts that were complementary to these mantle rocks is what can be gleaned from the polymict ureilites. These 17 (not accounting for many likely pairings) samples are regolith breccias, and contain a few percent feldspathic material (shown from O-isotopes to be indigenous to the UPB) in the form of small lithic and mineral clasts (Ikeda et al., 2000, 2003; Ikeda and Prinz, 2001; Kita et al., 2004, 2006; Cohen et al., 2004; Goodrich et al., 2004; Downes et al., in press). The recognition that these clasts represent a diversity of melt lithologies, none of which is strictly basaltic, pointed toward the possibility that melt extraction on the UPB was a fractional process (Cohen et al., 2004; Kita et al., 2004) and was one of the main motivations behind our work. In addition, these clasts have permitted the first precise dating of ureilites using short-lived radionuclide systems, yielding ages of ~5 Ma after formation of CAI (Goodrich et al., 2002a; Kita et al., 2003, 2007).

Goodrich et al. (2007) recognized that if melt extraction on the UPB was fractional, then it was important to examine the progress of smelting during the course of melting (as opposed to previous treatments of smelting in which the source region for each individual ureilite was assumed to have been “pre-smelted”). Thus, for a model bulk starting composition (given in Table 2 of that paper) we calculated (1) degree of melting, (2) the evolution of *mg*, (3) production

Table 1

Variation with depth, *D*, below the surface of lithostatic pressure, *P_s*, and acceleration due to gravity, *g*, in the UPB assuming a radius of *R* = 100 km and a mean density of $\sigma = 3300 \text{ kg m}^{-3}$.

<i>D</i> (km)	<i>P_s</i> (MPa)	<i>g</i> (m s ⁻²)
0.00	0.00	0.092
1.00	0.30	0.091
3.00	0.90	0.089
5.00	1.48	0.088
7.00	2.06	0.086
8.00	2.34	0.084
10.40	3.00	0.083
17.50	4.86	0.076
24.32	6.50	0.070
32.35	8.25	0.062
41.46	10.00	0.054
57.77	12.50	0.039
75.00	14.26	0.023
100.00	15.21	0.000

Table 2

Excess pressure, ΔP_1 , in melt as a function of mass %, *m_m*, and equivalent volume %, *q*, melted together with corresponding values of the critical length *L_c* (see text) and the vein length, *L_r*, required for the onset of vein growth.

<i>m_m</i> (%)	<i>q</i> (%)	ΔP_1 (MPa)	<i>L_c</i> (μm)	<i>L_r</i> (μm)
0.0100	0.0114	1.7	1596	175,318
0.0300	0.0341	5.1	1363	21,663
0.0500	0.0569	8.4	1189	8313
0.0700	0.0796	11.8	1055	4413
0.1000	0.1138	16.8	902	2232
0.1200	0.1365	20.2	823	1565
0.1503	0.1710	25.3	726	1000
0.1750	0.1991	29.4	663	733
0.2000	0.2275	33.6	609	555
0.2300	0.2616	38.6	555	411
0.2654	0.3019	44.6	502	300
0.3000	0.3412	50.4	460	227
0.4179	0.4752	70.1	357	100
0.5000	0.5686	83.8	309	61

of CO + CO₂ gas and (4) the evolution of mineralogy in the residue as a function of temperature for three different pressures (3, 6.5 and 10 MPa) on the UPB. The starting composition was determined from petrologic constraints following the approach of Goodrich (1999), and is similar to oxidized CV chondrites (all Fe assumed to be FeO) with the exception of having superchondritic Ca/Al ratio (2.5 × CI). The latter (which derives from the requirement to produce pigeonite, rather than orthopyroxene, as the dominant pyroxene) is assumed to be a post-accretionary feature, possibly established by mobilization of Ca during low-T aqueous alteration (Goodrich et al., 2002b, 2007).

Results of these calculations, which provide essential input for the present work, are summarized in Figs. 2 and 3. Two features deserve special note. First, these calculations show that although all ureilite source regions reach the silicate solidus at ~1050(±10) °C, and experience ~30% (± a few percent) total melting, their melting sequences vary greatly with depth because the temperature at which smelting begins (thus low-Ca pyroxene appears and CO/CO₂ starts to be produced) is strongly dependent on pressure. In the shallowest source regions, smelting begins nearly simultaneously with melting, whereas in the deepest it does not begin until ~22% melting has already occurred (notably, after plagioclase is exhausted), which has significant implications in the case of fractional, as opposed to batch, melt extraction. Second, these calculations confirm the result of Singletary and Grove (2003) that the UPB had an inverse temperature gradient; i.e. peak temperatures decrease from the shallowest to the deepest source regions.

2. THE SIZE OF THE UPB

As a prelude to calculations of the melting history and the extraction of melt from the UPB we first establish some basic physical constraints on the asteroid's properties. During the hydration and dehydration phases of its development, the asteroid must have lost a mass fraction corresponding to its initial ice mass fraction, say λ . It is easy to show, by considering the partial volumes of the compo-

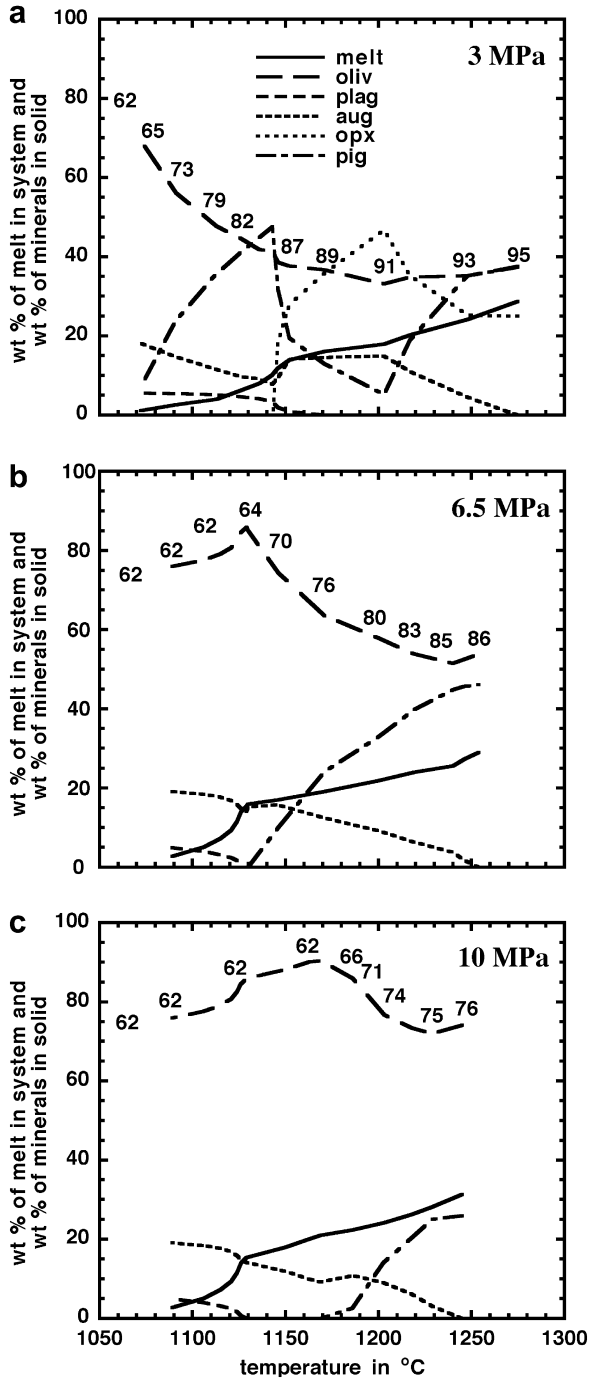


Fig. 2. Evolution of mineralogy and Fo (labelled on olivine curve) during progressive melting and smelting on the UPB at three different pressures (source region depths). All source regions reach the silicate solidus at $\sim 1050 \pm 10$ °C and experience $\sim 30\%$ total melting. However, their melting sequences vary significantly with depth because the temperature at which smelting begins (marked by the appearance of low-Ca pyroxene) is strongly dependent on pressure. Data from Goodrich et al. (2007). Oliv = olivine; plag = plagioclase; aug = augite; opx = orthopyroxene; pig = pigeonite.

nents, that as long as there is no significant change in the density of the bulk silicate component of the asteroid during the hydration and dehydration reactions, the ratio of

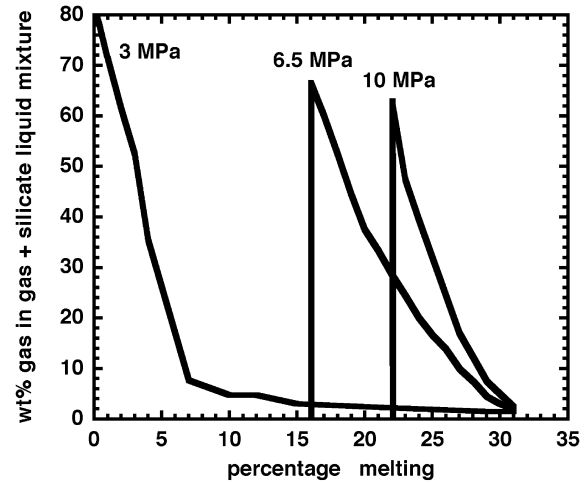


Fig. 3. Weight percent CO + CO₂ in gas plus silicate melt mixture as a function of degree of melting on the UPB at three different pressures (depths). The CO + CO₂ gas is a product of smelting and thus is not present until the onset of smelting (see Fig. 2). Data from Goodrich et al. (2007).

the final radius, r_f , of the asteroid after water loss to the initial radius, r_i , of the asteroid before ice melting is given by

$$r_f/r_i = \left[\frac{[(1-\lambda)\rho_i]}{[\lambda\rho_m] + [(1-\lambda)\rho_i]} \right]^{1/3} \quad (1)$$

where ρ_i is the density of ice, $\sim 917 \text{ kg m}^{-3}$ and ρ_m is the density of the silicate component, $\sim 3500 \text{ kg m}^{-3}$ appropriate to a CV-like composition. As an illustration, if the ice mass fraction λ takes the values 0, 0.1, 0.2 and 0.3, (r_f/r_i) has values 1.00, 0.89, 0.80 and 0.72. Thus, depending on the initial ice content, the asteroid may have experienced a significant decrease in size, but without an independent estimate of its initial ice content, which we do not have, we cannot specify how large this may have been. We can, however, place quite stringent constraints on the final size of the asteroid after these modifications have occurred, as follows.

We have meteorite samples that show evidence of having undergone $\sim 30\%$ (\pm a few percent) melting under pressure conditions ranging from ~ 3 to 10 MPa (± 1 MPa) (Goodrich et al., 2007, and references therein). Thus at the onset of silicate melting, the asteroid must have been large enough to allow a pressure of 10 MPa to be present in its mantle and small enough that rocks at the depth corresponding to 3 MPa pressure were heated sufficiently to be melted. We show in Table 1 the variation of lithostatic pressure, P_s , and acceleration due to gravity, g , with depth, D , in a body with a radius of $R = 100$ km and a mean density, σ , of 3300 kg m^{-3} (a typical density for peridotite). The relationships for a body with uniform density are

$$P_s = (2/3)\pi G\sigma(2DR - D^2) \quad (2)$$

and

$$g = (4/3)\pi G\sigma(R - D) \quad (3)$$

where G is the gravitation constant, $6.67 \times 10^{-11} \text{ m}^3 \text{ s}^{-2} \text{ kg}^{-1}$. The central pressure is proportional to the density and to the square of the radius.

The pressure range 3–10 MPa corresponds to depths of ~ 10 to ~ 50 km in a 100 km radius body and the central pressure is ~ 15 MPa; the acceleration due to gravity at the surface is 0.092 m s^{-2} . We will now show that the radius of the UPB could not have been much smaller, and is unlikely to have been much larger, than this 100 km value.

This involves considering the two major differences between the onset of silicate melting in the interior of an undifferentiated asteroid and the melting process inside a body like the Earth at its present stage of development. The first is the timescale of the process: the Earth is heated by long-lived radioisotopes of uranium, potassium and thorium with half-lives of ~ 4.5 , 1.2 and 14.1 Ga, respectively, whereas the asteroid is dominantly heated by short-lived ^{26}Al with a half-life of 0.72 Ma. More subtle is the fact that melting within the Earth is triggered by pressure release in the rising parts of convective systems, so that increasing degrees of partial melting take place under decreasing pressure and adiabatically decreasing temperature conditions, whereas in the asteroid, provided that bulk convection of the interior does not take place (an assertion that we justify later), melting is triggered purely by temperature increase. Thus as long as the ^{26}Al heat source is distributed uniformly, or at least randomly, throughout the asteroid, which we consider to be the most likely circumstance, the onset of melting occurs at all except the shallowest depths at essentially the same time. This is the consequence of the fact that, over a time interval t , the influence of radiative heat loss from the surface on the evolving internal temperature can only penetrate to a depth of $\sim (\kappa t)^{1/2}$, where κ is the thermal diffusivity of rock, $\sim 10^{-6} \text{ m}^2 \text{ s}^{-1}$ for all silicates. With t equal to a few Ma, the interval for which heat from ^{26}Al is available, this “skin depth” is less than ~ 10 km. The effect can readily be illustrated in more detail by calculating the temperature history for a spatially uniformly-distributed heat source within a spherical body using an analytical formulation like that given in section 95, Eq. (6), p. 207 of Carslaw and Jaeger (1947). Fig. 4 shows the variation of temperature with depth below the surface for the times at which temperatures of 1323, 1433 and 1543 K have been reached in the deep interior, these temperatures representing approximately 0%, 15% and 30% melting at the 3 MPa depth level (Fig. 2). Fig. 4 is plotted for an asteroid radius of 100 km, but the plot for a radius of 200 km would be indistinguishable at this scale: at a given depth temperatures differ by no more than 0.5% between these two asteroid sizes. Thus, essentially independent of its size, as an asteroid heats up its temperature will increase nearly uniformly at all depths below ~ 8 km, corresponding to a pressure of ~ 2.3 MPa (see Table 1). The very low temperatures in the shallower part of the asteroid are presumably the reason that no examples of ureilites with source region pressures much less than ~ 3 MPa (other than the polymict ureilite regolith breccias) are found, because these rocks would have resided in the cold outer shell. Furthermore, in a larger asteroid the 3 MPa level would be shallower. Thus in a 200 km radius asteroid the 3 MPa level would be at a depth of ~ 5 km, and the ~ 8 km level where the near-uniform internal temperature is reached would correspond to a pressure of

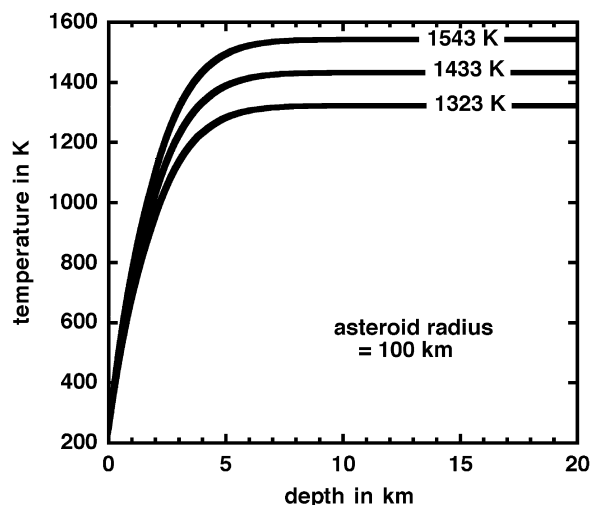


Fig. 4. The variation of temperature with depth in a 100 km radius asteroid at the times after formation when the deep internal temperature has reached 1323, 1433 and 1543 K. These temperatures correspond to $\sim 0\%$, 15% and 30% partial melting, respectively.

~ 4.8 MPa. Repeating this calculation for a range of asteroid sizes shows that if the 8 km depth is to correspond to a pressure of not more than 3 MPa then the asteroid cannot have a radius significantly larger than ~ 128 km. Note that the 8 km “skin depth” estimate used in this calculation would decrease if the thermal diffusivity of the outer layers were decreased, and this would lead to an increase in the estimate of the maximum asteroid radius, in proportion to the square root of the ratio by which the thermal diffusivity was decreased. Void-space creation during regolith formation on the surface of the asteroid could lead to such a decrease in thermal conductivity and hence in thermal diffusivity, though this would be partly offset by the corresponding decrease in bulk density and by the presence of ice in pore spaces as H_2O molecules diffused from the deeper interior. However, the amount of regolith formation on the timescales of a few Ma relevant here would be small (perhaps a few cm by comparison with the ~ 10 m of regolith formed in the lunar highlands during the first ~ 500 Ma of the Moon’s history) and we do not consider this effect to be important. Finally, we can also estimate the minimum asteroid radius: we have meteorites that experienced pressures of 10 MPa, which is the central pressure in an asteroid of radius ~ 82 km. Thus unless the asteroid radius was at least this large these meteorites could not exist. We adopt 100 km as the nominal UPB radius in what follows.

3. TIMESCALE FOR HEATING AND MELTING

The thermal history of the asteroid, assumed to accrete as a mixture of chondritic silicates and water ice (consistent with the suggestion that ureilite precursor material experienced pre-igneous aqueous alteration; Goodrich et al., 2002b), is modeled by following the progressive heating due to the decay of radioisotopes from an assumed initial temperature below the triple point of water. The treatment

is similar to that employed by Cohen and Coker (2000) to study hydration and dehydration in asteroids but the process is followed up to temperatures within the silicate melting range. We find that the thermal history is controlled almost entirely by the ^{26}Al content with a subsidiary contribution from ^{60}Fe . The inclusion or exclusion of all of the other radioisotopes considered by Cohen and Coker (2000) leads to a less than 1% change in the time at which a given amount of melting occurs. The assumption that ^{26}Al was alive at the time of ureilite formation is justified by the presence of excess ^{26}Mg in feldspathic clasts in polymict ureilites (Kita et al., 2003, 2007). The total Al content in the UPB is specified by assuming that it had a bulk composition similar to that given by Wasson and Kallemeyn (1988) for CV meteorites. The key parameters are then the ^{26}Al power production at CAI time, which for the assumed composition and the canonical $^{26}\text{Al}/^{27}\text{Al}$ ratio of 5×10^{-5} is nominally $2.156 \times 10^{-7} \text{ W kg}^{-1}$ of ice-free asteroid mass, and the ^{26}Al half-life, 0.720 Ma. We appreciate that the half-life has an uncertainty of $\sim 3\%$ and that the detailed chemical composition of the parent body is not actually known; the spread of compositions of CV meteorites, assumed to be representative of the UPB, is large enough that the power production rate is uncertain by at least 10%, but we adopt these nominal values. The corresponding heat contribution from ^{60}Fe is characterized by a nominal power production of $1.0 \times 10^{-8} \text{ W kg}^{-1}$ with a half-life of 1.04 Ma. All other contributing isotopes (see Cohen and Coker, 2000) have initial power production values at least three orders of magnitude smaller than ^{26}Al ; however, almost all of them have longer half-lives than both ^{26}Al and ^{60}Fe and thus contribute very slightly (at the $\sim 1\%$ level) to the late thermal history of melting after the ^{26}Al and ^{60}Fe are effectively exhausted.

Seven thermal stages are involved: heating of rock and ice to 273.15 K; buffering of the temperature at 273.15 K while ice is melting and the latent heat of 330 kJ kg^{-1} is supplied; heating of unreacted water and silicate reaction products while hydration is occurring between 273.15 and 300 K; heating of silicates until dehydration reactions begin at 530 K; heating of dehydration products until dehydration ends at 623 K; subsequent heating of dehydration products until the onset of silicate melting at 1323 K; and heating of unmelted silicates as melting progresses. During the hydration (273.15–300 K) and dehydration (530–623 K) phases, the latent heat of reaction (we use the 249 kJ kg^{-1} estimate from Cohen and Coker, 2000) is added to and subtracted from, respectively, the heat released by the radioactives to find the temperature rise, and it is assumed that the latent heat transfer occurs uniformly across the relevant temperature interval. Similarly, it is assumed that during silicate melting the latent heat required (taken as 400 kJ kg^{-1}) is absorbed uniformly across the solidus–liquidus temperature range, though in this case the actual melting temperature range varies with pressure (and hence depth), due to the compositional (mg) variation caused by smelting: although the solidus temperature is the same (1323 K) at all pressures because it is reached before smelting begins (Fig. 2), the liquidus temperatures at 3, 6.5 and 10 MPa are 1860, 1842 and 1827 K, respectively (these are

obtained from MAGPOX for the pre-smelted $mg \sim 91$, $mg \sim 86$ and $mg \sim 76$ compositions – see Goodrich et al., 2007).

The thermal history is traced using time steps of 0.5 ka before silicate melting begins and 1 ka afterwards. Converting the available heat into a temperature rise during each of the thermal stages involves summing the heat per unit mass produced locally from all of the isotopes, subtracting or adding the latent heat per unit mass where relevant, and dividing the result by the weighted mean specific heat at constant volume of whichever materials (ice, water and/or silicates) are present at the current temperature. During melting and smelting it is also necessary, as described in detail later, to take account of advective redistribution of heat as silicate melt and volatiles are transferred to shallower levels or erupted. The temperature-dependent specific heats of ice and water were taken from standard sources, and for the silicates a weighted average of the specific heats of the mineral assemblages present was used. Above the solidus these are dominated by olivine, augite, pigeonite and plagioclase as shown in Fig. 2, and data for these were taken from a compilation by Dobran (2001); there is not a great variation of specific heat with composition for silicates and so the data for the same minerals were used at lower temperatures. Fig. 5 shows the variations of the specific heats with temperature.

Both the water vapor released during dehydration and the gases (mainly carbon dioxide and hydrogen) released by the earlier, lower-temperature hydration reactions are assumed to escape efficiently through fractures to the surface. These fractures will have been generated by the build up of gas pressure as the reactions proceeded. It has been proposed that, in extreme cases, gas generation during hydration reactions may have led to massive disruption and even dispersal of some small asteroids (Wilson et al., 1999). However, the $\sim 100 \text{ km}$ radius of the UPB was sufficiently larger than the $\sim 35 \text{ km}$ radius marking the upper size of body that can be disrupted in this way (Wilson et al., 1999) that neither of the gas production phases led to disruption, but both must have contributed to the formation

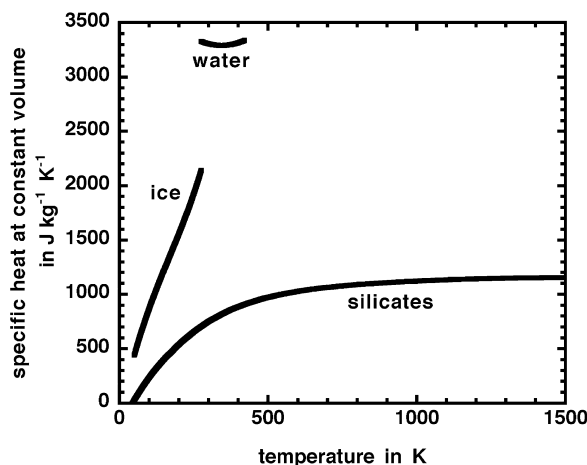


Fig. 5. The variation with absolute temperature of the specific heats at constant volume of ice, liquid water and the average silicate assemblage in the UPB.

of a network of fractures in the asteroid. This network may have been at least partially removed in the deep interior of the asteroid by the annealing effects of the high temperatures as silicate melting was approached, but it will have survived in at least the cooler outer $\sim 5\text{--}7$ km of the asteroid (see Fig. 4) to be exploited by the silicate melts, and even in the deep interior the pressures are low enough that the annealing process would not have been very efficient.

The transfer of melts out of the interior of the asteroid during silicate melting plays a key role in its thermal history since most of the Al in the rock is contained in plagioclase, a mineral that is completely consumed during the melting process (Fig. 2). Hence the main heat source is progressively removed from the asteroid interior. We show below in Section 5.1 that the large volume fraction of carbon monoxide produced by the smelting reaction causes much of the melt to be lost to space in explosive eruptions. However, the fraction that is not lost is intruded into the shallow crustal layers where it plays a key role in controlling the temperature history at the 3 MPa pressure level. This retained melt fraction is denoted f_i and is a model parameter for which we solve.

We model the spatial variations of properties within the asteroid by dividing it into five zones: these are the region from the surface down to 7.0 km depth, representing the cold crust; the layer from 7.0 to 17.1 km, taken to be representative of the 3 MPa pressure level at 10.4 km (see Table 1); the layer from 17.1 to 32.3 km, representative of the 6.5 MPa pressure level at 24.3 km; the layer from 32.3 to 57.8 km, representative of the 10 MPa pressure level at 41.5 km and ending at the 12.5 MPa level where smelting ceases; and the spherical region between 57.8 km depth and the center. The volumes of these spherical shells are 8.20×10^5 , 9.80×10^5 , 10.92×10^5 , 9.82×10^5 and 3.15×10^5 km³, respectively.

At each time step in the model we use the temperature increase to define the increment of melting at each of the 3, 6.5 and 10 MPa pressure levels (Fig. 2; see also Fig. 7b of Goodrich et al., 2007). The melting in the central spher-

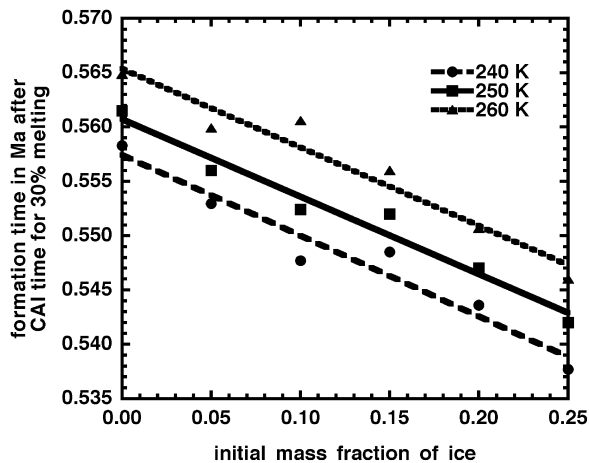


Fig. 6. The time after CAI formation at which the UPB must accrete in order to achieve 30% melting in the interior. Values are shown for plausible ranges of the initial mass fraction of ice and the temperature at accretion.

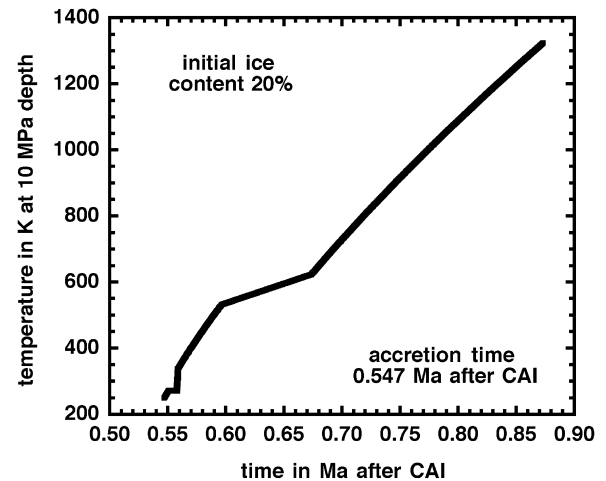


Fig. 7. The temperature at the 10 MPa depth in the UPB as a function of time after CAI formation as the asteroid heats up to the onset of silicate melting. This example assumes that the asteroid accretes 0.547 Ma after CAI with an initial temperature of 250 K and contains 20% ice by mass.

ical region is assumed to follow the melting sequence calculated for primitive ($mg \sim 62$) UPB precursor material (Goodrich et al., 2007), with no smelting. We track the Al removal using polynomials fitted to the plagioclase contents as a function of melt fraction (Fig. 2). At each time step, the heat source due to ^{26}Al at each of the three pressure levels in the asteroid interior is scaled down in proportion to the currently remaining plagioclase mass fraction. The fraction f_i of retained melt is inserted into the crust to form a growing intrusion layer (i.e. a sill) centered on a depth of 7 km, essentially the base of the outer layer that never undergoes melting as the asteroid warms up. At each time step, the new average Al content of this intrusion is calculated from its previous Al concentration and the Al content of the newly added volume. The consequence of the evolving compositional difference between the melt and its source rocks is that as melting in the source region progresses from zero to 30%, the ^{26}Al content of the melt in the intrusion decreases from $\sim 85\%$ to $\sim 42\%$ of the initial ^{26}Al content in UPB parent material. A corresponding tracking of the Fe shows that as melting progresses the ^{60}Fe content of the intrusion increases slightly from 1.05 to 1.09 times the initial value in the parent material. The heat from the growing intrusion that is conducted upward toward the surface is considered in Section 5.4 where it is used to model the cooling history of the sill contents. The presence of the sill heat source greatly reduces heat transfer from deeper levels, and plays a major role in controlling the maximum degree of melting at the 3 MPa level.

As smelting progresses at any given level, the metallic iron that is produced is assumed to settle downward. The process is not modeled here in detail but is likely to be complex. For example, droplets of immiscible liquid metal produced at smelting sites may be locally so small that they are initially carried upward in the surrounding silicate melt but, being so much denser (~ 7200 kg m⁻³), they will always have significant downward terminal velocities, and so in

the narrowest melt veins, where the silicate melt speed is very small, they will have the opportunity to coalesce into larger droplets with larger terminal velocities and must eventually migrate downward. As an extreme example, if all of the iron coalesced into a central metal core, this would have a radius of ~ 41 km occupying $\sim 7\%$ of the volume of the UPB. The redistribution of mass would lead to a negligible change in asteroid radius but would cause the central pressure to rise progressively from its initial value of 15.2 MPa to 26.6 MPa. However, the effect on the pressures within the 3–10 MPa range of levels from which the ureilite meteorites are derived would be much less dramatic. The rearrangement of materials with the UPB would mean that silicates that completed their melting in equilibrium with a pressure of 10 MPa would in fact have begun melting at a slightly greater depth in the asteroid where the ambient pressure was 10.95 MPa. The pressure changes at shallower levels would be proportionally smaller. Since we are in any case using the melting process at 10 MPa (and at 6.5 and 3 MPa) to approximate conditions over a range of asteroid radii, spanning about a 20% pressure range in each case, we can safely neglect this effect.

A final issue concerns the approximate method used to model the temperature distribution within the asteroid. We have not solved the full heat diffusion equation numerically; this would be particularly complicated in the present case where heat is being advected (by moving melt), as well as conducted, through the asteroid. Instead, we approximate the evolving temperature gradient in the crust as the difference between the intrusion temperature and the surface temperature (assumed to be maintained at the initial formation temperature) divided by the depth of the intrusion to find the total amount of heat lost by conduction to the surface in each time step. We divide this by the current total mass of the asteroid to obtain a heat loss per unit mass. This is then subtracted from the heat per unit mass generated by radioactive decay at all levels within the asteroid. Next, we examine the new temperatures at all depths after this first-order heat transfer adjustment and refine them by allowing heat to be conducted between each of the three pressure levels, the crustal intrusion and the central region of the asteroid as a function of the temperature change that has occurred and the length of the time step.

The target for a successful run of the model is that 30% melting should be achieved at each of the 3, 6.5 and 10 MPa pressure levels. As a separate phase in obtaining solutions to the model for a given set of input parameters we experimented with optimizing the value used for the thermal conductivity during the second temperature adjustment phase. We find that a value larger than the actual thermal conductivity (expected to be close to $2 \text{ W m}^{-1} \text{ K}^{-1}$ at the temperatures involved), by a factor of close to 6 is needed for two reasons: one is the crude way the temperature profile is being specified (we are effectively approximating a smooth profile by five data points: the temperatures at the three internal pressure levels, the crustal intrusion and the surface), and the other is the fact that some heat is being advected through the system by the melt migration. We optimize this thermal conductivity factor simultaneously with optimizing the value of f_i , the fraction of melt that is re-

tained in the sill. The optimum value of f_i is found to be 0.147, implying that $\sim 15\%$ of the melt is not lost to space.

The thermal calculations were implemented as a FORTRAN program that was used to explore the variation of the melting history with the key controlling parameters: the time of asteroid formation after CAI time, the initial temperature, and the initial ice content. The outputs generated are the times at which the temperature reaches a given value during the warm-up to melting; the times and temperatures at which successive increments of partial melting occur at each of the 3, 6.5 and 10 MPa pressure levels; and the temperature history of the melt intruded into the crust. The time of onset of melting is the same at all depths, given our earlier demonstration of the near-uniform temperature at depths greater than ~ 8 km and the fact that the solidus temperature is independent of pressure over the small pressure range considered. However, the time to reach a given degree of partial melting does vary with depth due to the depth-dependence (i.e. *mg*-dependence) of the liquidus.

The most important input parameter controlling the thermal history is, as expected, the time of formation, though initial temperature and ice content also have strong influences. Consideration of the measured temperatures of main belt asteroids (Lim et al., 2005) suggests that a plausible accretion temperature was ~ 250 K, and measurements of the density of the large asteroid Ceres (McCord and Sotin, 2005) imply that the present-day, and probably initial, H_2O content was less than 30% by mass. Using these values as order of magnitude guides, we show in Fig. 6 the variation of the time at which the asteroid must be formed to achieve 30% silicate melting at the 10 MPa depth level as a function of the initial ice mass fraction in the range 0–30% and the asteroid formation temperature in the range 240–260 K. Given that we do not in fact know how far from the (then less luminous) Sun the UPB accreted, lower model accretion temperatures might be justified, and Fig. 6 shows that these would drive the required formation time toward earlier times. However, the implication of the starting conditions adopted here is that the asteroid accreted between ~ 0.535 and ~ 0.565 Ma after CAI formation. We note that this result is similar to the <1 Ma accretion time of Bizzarro et al. (2005) and the 0.75 Ma accretion time of Hevey and Sanders (2006) for planetesimals in our solar system, but differs significantly from the 2–3 and 2.1–2.5 Ma results of Sahijpal et al. (2007) and Kita et al. (2005), respectively. There are various reasons for these differences: e.g. no loss of melt to space in the case of Sahijpal et al., and the onset of convection at $\sim 50\%$ melting due to no loss of melt in the case of Hevey and Sanders. However, these comparisons serve to stress the importance of defining a detailed self-consistent history for the thermal evolution of a particular body. The major difference between the model presented here and these other treatments is the detailed tracking of the removal of the melt from the interior and the specification of its final fate.

Based on Fig. 6 we choose an accretion temperature of 250 K, an ice content of 20%, comparable to the values used by Cohen and Coker (2000), Young et al. (1999) and Young (2001), and a formation time of 0.547 Ma after CAI for subsequent illustrations. The canonical $^{26}\text{Al}/^{27}\text{Al}$ ratio

was decreased from its value at CAI time using the 0.72 Ma half-life to provide the heat production rate at the time of formation. Fig. 7 shows the temperature as a function of time up to the onset of silicate melting and Fig. 8 shows the entire temperature history at all three internal pressure levels and in the melt intruded into the crust treated as a global sill. Finally, Fig. 9 shows how the melt fractions in the interior vary with time. Clearly a maximum amount of melting very close to 30% is achieved at all pressure levels, although the time at which this happens varies between ~ 4.5 and ~ 5.8 Ma after CAI. We emphasize again that achieving the requisite high temperatures (thus 30% melting) in the shallowest source regions depends critically on the presence of the sill, a result that was foreseen by Kita et al. (2005).

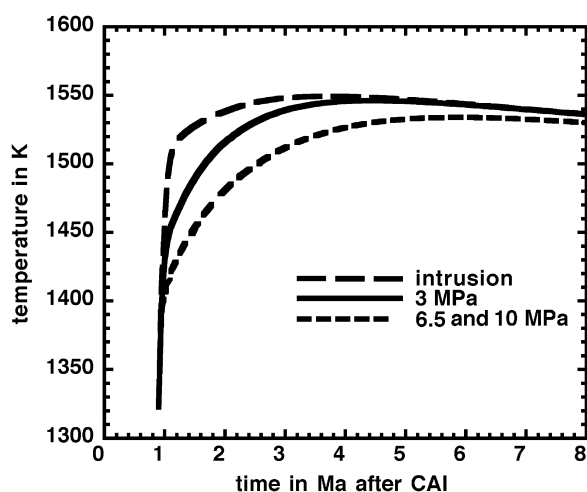


Fig. 8. The temperature at various pressure levels (i.e. depths) in the UPB as a function of time after CAI formation. The temperature histories at the 6.5 and 10 MPa levels are sufficiently similar that they are indistinguishable on this plot. Accretion conditions are the same as for Fig. 7.

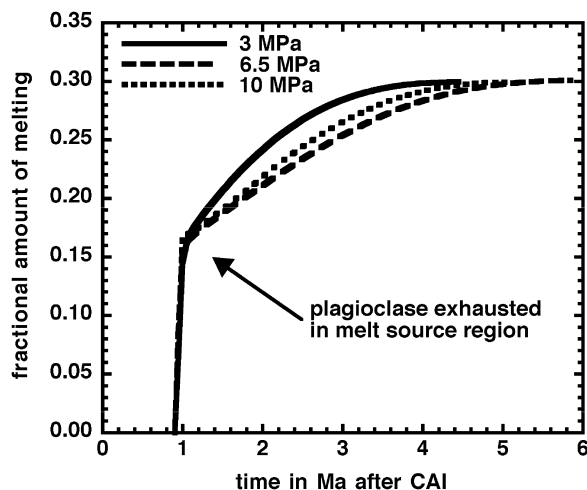


Fig. 9. The fractional amount of melting that occurs at the 3, 6.5 and 10 MPa pressure levels in the UPB as a function of time after CAI formation. Accretion conditions are the same as for Fig. 7.

Fig. 9 can be used to find the rate of melt production, ϕ , at each pressure level as a function of time. Fig. 10 shows the result: the main feature, controlled by the half-life of ^{26}Al , is the dramatic decrease in melt production rate from values in excess of $100 \text{ m}^3 \text{ s}^{-1}$ in the very early stages of melting at ~ 1 Ma after CAI to values of $\sim 5 \text{ m}^3 \text{ s}^{-1}$ between 2 and 3 Ma after CAI, decreasing again to extremely small values as the end of melting is approached beyond 5 Ma. The significance of this for melt extraction is explored in the following section. Here, we point out that the bulk of the melt is produced quickly in the early stages of melting, before plagioclase is exhausted. The implication of this, which we will examine later, is that the melts that produced the indigenous feldspathic clasts in polymict ureilites were produced in a short period of time at ~ 0.9 –1 Ma after CAI.

4. MELT FORMATION AND EXTRACTION FROM THE ASTEROID INTERIOR

The onset of melting in asteroids, just as in the Earth, involves the formation of melt films along grain–grain contacts and subsequent melt migration. This can occur by percolation of melt along grain boundaries (Maaloe and Schie, 1982; McKenzie, 1984; Richter and McKenzie, 1984; Spiegelman and Elliot, 1993; Kelemen et al., 1997) and by compaction of the unmelted matrix, either in a monotonic fashion (Sleep, 1974; McKenzie, 1984; Richter and McKenzie, 1984; Ribe, 1985; Spiegelman and McKenzie, 1987) or by the formation of propagating waves of variation in porosity (Scott and Stevenson, 1984, 1986). Various papers address the collection of melt into veins on a larger scale than the fabric size (i.e. the mineral grain size) of the unmelted matrix (Maaloe, 1981; Spence et al., 1987; Sleep, 1988; Hart, 1993; Maaloe, 2003) and the further interconnection of large veins to form the dikes which ultimately drain large volumes of partial melt to the surface (Nicolas and Jackson, 1982; Sleep, 1984; Fowler, 1985; Nicolas, 1986; Wickham, 1987; Sleep, 1988). We incorporate

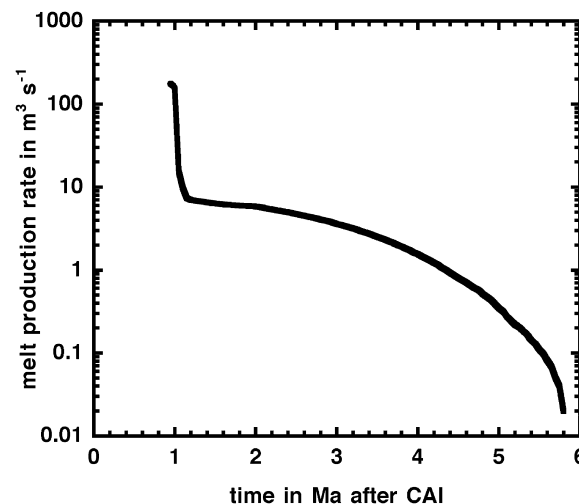


Fig. 10. The total silicate melt production rate in the UPB as a function of time after CAI formation. Accretion conditions are the same as for Fig. 7.

key aspects of these treatments into a model of melt extraction from the UPB as follows.

All of the treatments developed for the Earth relate to conditions within it at the present time, with the spatial and temporal scales of the melting system set by mantle dynamics driven by the current heat loss rate and temperature structure of the planetary interior. Strain rates are sufficiently small that large deviatoric stress do not build up easily and cannot be sustained for geologically long periods. [Maaloe \(2003\)](#) gives a calculation for melting beneath mid-ocean ridges on Earth showing that magma produced by 24% partial melting of mantle rock would reflect the rise of the host material between pressure levels of 5.6 and 3 GPa, corresponding to depths between ~ 170 and ~ 90 km. The ~ 80 km rise would occur at a speed of ~ 0.1 m/a implying a time interval of ~ 0.8 Ma. The ambient temperature of the host rocks would decrease from ~ 1500 to ~ 1300 °C over this depth range and the effective viscosity of the host rocks (a function of both the bulk and shear viscosities) would be $\sim 10^{18}$ Pa s ([Sleep, 1988](#)). In contrast, in the UPB the time required to reach $\sim 24\%$ partial melting after the onset of melting would be between ~ 1 and 2 Ma ([Fig. 9](#)), up to double the terrestrial value. However, because the UPB was much smaller than the Earth, internal lithostatic pressures were also much smaller ([Table 1](#)) so that melting started at a lower temperature ([Fig. 2](#)), 1323 K to be compared with ~ 1620 K in the Earth's mantle ([Turcotte and Schubert, 2002](#)). This means that the unmelted matrix would probably have had a somewhat higher effective viscosity than the Earth's mantle on the point of melting. Given [Sleep's \(1988\)](#) suggested value of $\sim 10^{18}$ Pa s for partially molten mantle in the Earth and [Spiegelman's \(1993a\)](#) suggested range of 10^{18} – 10^{19} Pa s, we adopt 3×10^{18} Pa s for the UPB. We show below that this higher viscosity approximately compensates for the slower rate of melting in controlling the relaxation of the excess melt pressures induced by the volume increase on initial partial melting, and the presence of high melt pressures would have assisted the interconnection of growing melt veins. Some aspects of this behavior were addressed by [Muenow et al. \(1992\)](#) and [Keil and Wilson \(1993\)](#) in modeling the removal of mafic mantle melts and Fe,Ni,S core-forming fluids from asteroid parent bodies, but the treatment given below is more detailed in that it relates the onset of melt extraction to the mineralogy and the degree of partial melting, the key factors in understanding the chemistry of the melts.

4.1. Geometry of melting

Consider an array of mineral grains ([Fig. 11](#)), each assumed to be a uniform cube of size L (the exact geometry adopted is not critical). When more than one mineral species is present, melting may occur only at the interfaces between some fraction of the minerals, and we idealize this by assuming that if a grain is melting then melt forms at all 12 of its edges, as shown, but that only a fraction f of the grains are in this state. The cross-sectional area A of any one melt vein of diameter α is

$$A = (\pi/4)\alpha^2 \quad (4)$$

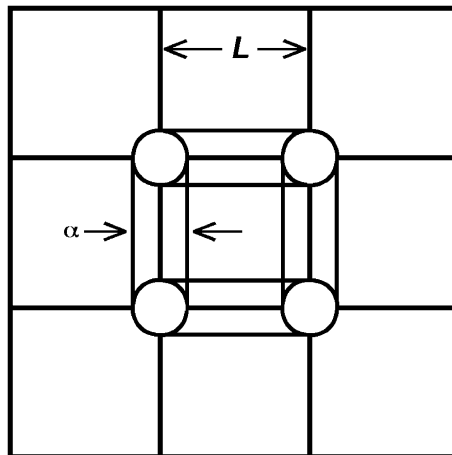


Fig. 11. Geometry of a cubic mineral grain that is melting along all 12 of its edges while in contact with other grains of similar shape that are not melting.

The volume V_{vein} of one vein is

$$V_{\text{vein}} = (\pi/4)\alpha^2 L \quad (5)$$

and the volume of all 12 veins is $3\pi\alpha^2 L$. However, each vein is shared by 4 adjacent grains, so the melt volume corresponding to one grain is

$$V_{\text{melt}} = (3/4)\pi\alpha^2 L \quad (6)$$

Since a fraction f of all of the mineral grains is melting, and the volume of one mineral grain is L^3 , this melt volume occurs in a reference volume V_{ref} equal to (L^3/f) , and so the melt volume fraction q is given by the ratio $(V_{\text{melt}}/V_{\text{ref}})$, i.e.

$$q = (3f\pi\alpha^2)/(4L^2) \quad (7)$$

The number of veins per unit volume, $N = (q/V_{\text{vein}})$, is

$$N = 3f/L^3 \quad (8)$$

and the average distance, d , between veins is equal to $(1/N)^{1/3}$ so that

$$d = L/(3f)^{1/3} \quad (9)$$

Thus the ratio r between the average separation d and the mineral grain scale length L is

$$r = (3f)^{-1/3} \quad (10)$$

[Fig. 12](#) shows this relationship, and clearly many veins will be in close proximity, i.e. $r < 1$, if f is greater than ~ 0.2 – 0.3 whatever the detailed geometry. At the onset of melting, the UPB contained three major mineral species, and at the start of melting augite and plagioclase, totaling 25% of the rock, were melting together, so we adopt $f = 0.25$ and infer that close proximity between melting veins would have been very common.

4.2. Melt pressure

We next estimate the likely pressures in pockets of melt trapped between mineral grains as a function of the amount of melting that takes place and show how this rapidly

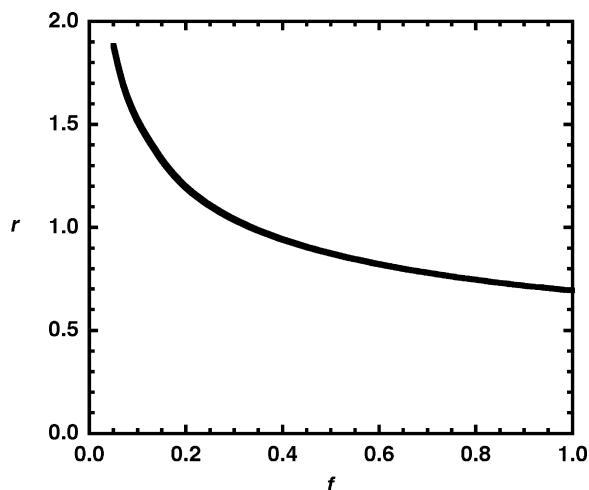


Fig. 12. The variation of the ratio r of the average melt vein separation d to the mineral grain scale length L as a function of the number fraction of all of the mineral grains that are melting, f .

encourages increased connectivity between melt veins if none already exists. Following Muenow et al. (1992), we adopt a convenient geometry by modeling the melting grains as spheres, each having an initial radius x_0 and uniform density ρ_s , which melt to form a liquid of density ρ_l . At some general time, melting has progressed inward from a grain surface to some radius x , so that the current melt volume is $[(4/3)\pi(x_0^3 - x^3)]$, and the pressure in the liquid phase is P_l . If a pressure increase dP_l accompanies an inward increase dx in the radius of the melt zone, then

$$4\pi x^2 dx (\rho_s / \rho_l) = (4/3)\pi(x_0^3 / f)(dP_l / \mu) + (4/3)\pi(x_0^3 - x^3)(dP_l / \beta) \quad (11)$$

Here, the left hand side is the volume increase due to conversion of a volume element of the solid to lower density liquid. The first term on the right hand side is that part of the volume increase accommodated by compression of the surrounding matrix, taking account of the fact that only a fraction f of the grains are melting, and the second term is that part taken up by compression of the liquid itself, μ and β being the bulk moduli of the unmelted grains and the liquid, respectively (Tait et al., 1989). Note that this treatment assumes that only a liquid phase is produced on melting. As noted in Section 1, gas production by smelting eventually occurs at all depths in the UPB down to the 12.5 MPa pressure level. Gases are much more compressible than liquids and so the presence of gas will reduce the rate at which the pressure rises with increasing melt fraction. However, it is only in the shallowest regions undergoing melting that any gas is produced very early in the melting process. We shall shortly show in Section 4.3 that a fully-connected vein network is likely to be generated after as little as 0.15% melting, and the calculations underlying Fig. 2 imply that only within a layer about 100 m thick at the ~ 3 MPa pressure level at a depth of 10–11 km will gas be present during the period of vein connection. Since a complex vein and dike network will already have evolved in the deeper interior by this time (melting

starts first in the deepest parts of the asteroid as will be discussed in detail in Section 5.2), fractures will be propagating into the 100 m thick layer from below as well as being generated within it. We therefore feel justified in neglecting the details of this process.

Eq. (11) is readily integrated to give the pressure increase in the melt, ΔP_l , in excess of the lithostatic load P_s , as

$$\Delta P_l = (\rho_s / \rho_l) \beta \ln \left[1 + (f\mu / \beta) (1 - \{x/x_0\}^3) \right] \quad (12)$$

Since only a fraction f of the mineral grains is melting, the volume fraction of melt, q , in the entire mineral assemblage is by definition equal to $[(4/3)\pi(x_0^3 - x^3)f] / [(4/3)\pi x_0^3] = f(1 - \{x/x_0\}^3)$, and so Eq. (12) can be written

$$\Delta P_l = (\rho_s / \rho_l) \beta \ln [1 + (\mu / \beta) q] \quad (13)$$

Appropriate values of β and μ are 10 and 13 GPa, respectively (Muenow et al., 1992). With a melt density of $\rho_l = \sim 2900 \text{ kg m}^{-3}$ and a matrix density ρ_s initially equal to the bulk density of the asteroid, $\sigma = \sim 3300 \text{ kg m}^{-3}$, $(\rho_s / \rho_l) = \sim 1.14$, the pressure increase ΔP is shown in Table 2. Values are given in terms of the mass fraction of melt, m_m , which is related to the volume fraction of melt, q , by

$$m_m = (q\rho_l) / [(1 - q)\rho_s + q\rho_l] \quad (14)$$

and the corresponding values of q are also listed. Clearly, initial pressures of a few to a few tens of MPa are possible even at small amounts of melting when melt is completely trapped between bonded mineral grains. However, we now show that these pressures rapidly lead to connections forming between melt pockets.

4.3. Vein connection

The mineral grain fabric scale in the UPB prior to melting, and hence the typical length, L , of the initial melt veins, is likely to be similar to that of chondritic meteorites that experienced high-temperature metamorphism but no silicate melting, or to that of the most primitive achondrites. We therefore expect that L will lie in the range 100–300 μm (Brearley and Jones, 1998; Mittlefehldt et al., 1998). Although, as we showed above, the initial melt veins are likely to be in close proximity, their degree of interconnection will increase greatly if the stresses at the tips of veins become large enough to allow them to fracture the unmelted host matrix. A detailed discussion by Rubín (1993) shows that the criteria for this to occur are best expressed by requiring a balance between the external lithostatic load, P_s , the total internal melt pressure, $(P_s + \Delta P_l)$, and the grain–grain cohesive forces represented by the tensile strength, S . In the present notation, and removing Rubín's assumption that the veins are much larger than the mineral grain fabric, since this is not true at the scale of the veins we are considering, the stress balance defining the vein length L_f at which fracturing will just occur is given by

$$\Delta P_l (L_f + L_c)^{1/2} = (8^{1/2} / \pi) (\Delta P_l + P_s + S) L_c^{1/2} \quad (15a)$$

resulting in

$$L_f = \{ (8/\pi^2) [(\Delta P_l + P_s + S) / \Delta P_l]^2 - 1 \} L_c \quad (15b)$$

where L_c is a critical length given by

$$L_c = (\pi/4)[\varepsilon/(1 - \nu)][\delta_c/(\Delta P_1 + P_s + S)] \quad (16)$$

Here, ε and ν are the shear modulus and Poisson's ratio, respectively, of the unmelted mineral grain matrix and δ_c is the maximum distance over which grain–grain cohesive forces can act. In partially molten rock under relatively low confining loads (the ~ 10 MPa stress-level depth in the UPB is the equivalent of 400 m depth on Earth), the value of $[\varepsilon/(1 - \nu)]$ is probably ~ 4 GPa, the value found by Parfitt (1991) for dikes propagating within Kilauea Volcano, Hawai'i; this is much less than the commonly cited values of order 30 GPa (Rubin, 1993) for the deeper lithosphere on Earth. Experimental measurements on unfractured rocks suggest that δ_c is ~ 10 μm (Ingraffia, 1987) and that S is ~ 10 MPa (Ingraffia, 1987; Jaeger and Cook, 1979). Using $P_s = 80$ bars as an average value of the 30–125 bar range of lithostatic loads in the ureilite rocks, Table 2 shows how L_c and hence L_f vary with the amount of melting. Examination of the values of L_f shows that at the lower end of the expected range of grain lengths, $L = 100$ μm , as about 0.48 volume % melting would have to occur to initiate vein tip fracturing; at the upper end of the expected length range, $L = 300$ μm , the process would begin at ~ 0.30 volume % melting; and if any grains 1000 μm , i.e. 1 mm, long were present, only ~ 0.17 volume % melting would be required. Eq. (7) can be used to find the diameters of the veins assuming the tubular geometry of Fig. 11. The diameter, α , of a 100 μm vein at 0.48 volume % melting is ~ 4.5 μm ; the corresponding values are ~ 10.7 μm for a 300 μm long vein at $q = \sim 0.30$ volume % melting and 26.9 μm for a 1 mm long vein at 0.17 volume % melting.

As soon as one unusually large vein begins to grow, it has a large probability of intersecting other veins, and it seems safe to assume that rapid interconnection between pockets of melt trapped between grains will occur after about 0.15 volume % melting is reached, with typical vein lengths of ~ 1 mm and widths of ~ 25 μm , and we adopt these values for subsequent use. Note that Table 2 implies that this degree of melting would induce about a 25 MPa pressure in the melt. This would mean that this initial fracturing phase would occur with much higher melt pressures than the lithostatic pressures in the UPB, well above the ~ 12.5 MPa pressure above which smelting cannot occur. Thus the very earliest isolated melt pockets would be gas-free everywhere. However, as soon as vein interconnection became common, the entire asteroid interior would expand very slightly (by $\sim 0.05\%$) to accommodate the volume increase on melting and the pressures at all depths in both melt and matrix would quickly relax to lithostatic, with the combination of melting and smelting appropriate to each depth then being resumed. We note that it is possible that the inherent strength of the metamorphosed UPB interior may have been less than that of unfractured rocks from the Earth's interior; however, reducing the assumed inter-grain tensile strength by a factor of 2, from 10 to 5 MPa, only reduces the pressure (and melt fraction) at which fracturing begins by $\sim 15\%$.

A further aspect of the metamorphic history of the UPB is the possibility that fractures formed during the hydration

and dehydration phases of heating were not completely annealed by the onset of silicate melting but remained as closed but weak incipient fractures. In that case, the 30 MPa melt pressure would apply only to melt completely trapped between bonded grains. As soon as pressurized melt pockets became connected to these weak relict fractures they would utilize them in preference to creating new fractures, and so both the timescale and the preponderance of excess pressures needed for production of a thoroughly interconnected fracture network would be less.

4.4. Evolution of vein network

The way in which the size spectrum of the pathways in an interconnected network develops in a region of partial melting is poorly understood. Recent work by Valentini et al. (2007) suggests that beneath mid-ocean ridges on Earth fracture networks on scales between millimeters and meters are 4–5 times more efficiently interconnected than a random arrangement of fractures would be. The presence of high-temperature planar dikes in ophiolite exposures of mantle peridotites (Nicolas and Jackson, 1982) strongly suggests that vein networks can evolve into much larger-scale dikes in such regions, and this led Sleep (1988) to propose mechanisms for the evolution of vein networks in which melt moves from smaller veins into progressively growing larger ones as a result of pressure gradients driven by differences in the principle stresses. Keil and Wilson (1993) explored a melt migration process of this kind for small asteroids. One relevant complication is that as soon as an interconnected vein network is in place throughout the region of melting, so that melt can begin to move, new processes influence the scales at which melt segregation occurs. Various instabilities may develop within the region of partial melting, driven by small inhomogeneities in density and porosity. Density variations will induce Rayleigh–Taylor instabilities, potentially able to grow into convection cells (though we show shortly that they do not develop this far). Porosity variations will grow and become concentrated, with zones of higher than average porosity traveling upward as solitary waves (commonly called magmons) that can propagate faster than the melt is rising through the unmelted matrix (Spiegelman, 1993b). The factor controlling porosity fluctuations is the compaction length, δ , given by

$$\delta = \{k[\zeta + (4/3)\xi]/\eta\}^{1/2} \quad (17)$$

where ζ and ξ are the bulk viscosity and shear viscosity of the matrix, respectively, both taken as 3×10^{18} Pa s based on the temperature at which melting begins, as discussed earlier, and η is the viscosity of the melt, taken as 1 Pa s. The quantity k is the permeability, given by

$$k = (Y^2 q^a)/b \quad (18)$$

where Y is the fabric scale, dictated by vein lengths so that $Y = \sim 1$ mm, q is porosity of the system, equal to the local melt fraction, which by definition is at least equal to the threshold melt volume fraction for vein interconnection, found above to be ~ 0.002 , and a and b are constants. Various treatments of the geometry of melt vein systems (e.g. von Barga and Waff, 1986) suggest that a lies between 2

and 3 and b between 100 and 3000. An analysis by [Turcotte and Schubert \(2002\)](#) for a cubical array like that of [Fig. 11](#) gives $a = 2$ and $b = (72 \pi) = \sim 226$. Inserting these values we find $k = \sim 1.77 \times 10^{-14}$ which in turn implies $\delta = \sim 350$ m. [Spiegelman \(1993b\)](#) showed that the size of the propagating solitary waves of melt concentration is of the same order as (and probably a little larger than) δ . Thus, although melting is occurring simultaneously over a large vertical distance within the asteroid, there may be small variations in melt content within regions with this vertical extent.

There is some ambiguity about the typical horizontal scale of melt concentration variations. This could be taken as the wavelength ω of density-driven Rayleigh–Taylor convective instabilities present in the melt zone, given by

$$\omega = 1.284X \quad (19)$$

where X is the characteristic vertical extent over which significant density differences exist. At one extreme this might be taken as the entire vertical extent of the region within which melting is taking place, equal to the radius of the asteroid minus the thickness of the outer shell that is conductively cooled, ~ 10 km, so that $X = \sim 90$ km and $\omega = \sim 120$ km. This would make the area of the potential convection cell $\sim [\pi(\omega/2)^2] = \sim [\pi 60^2] = 11,000 \text{ km}^2$. For melt being extracted from a region half way between the center and the surface of the asteroid, where the area of a spherical shell is $[4\pi 50^2] = 31,400 \text{ km}^2$, this implies that there will be only about 3 such unstable regions active at any one time; nearer the surface, where the area of a shell approaches $[4\pi 90^2] = 101,800 \text{ km}^2$, there could be ~ 10 such regions at any one time and deep within the asteroid only one or two. However, it could be argued that density variations are also present on the scale of the porosity solitary waves, in which case with $X = \delta = \sim 350$ m, ω will be ~ 450 m and the typical area of a region from which melt is being expelled $[\pi(\omega/2)^2]$ will be $\sim 0.16 \text{ km}^2$. In this case $\sim 200,000$ extraction events could be occurring within the asteroid at any one time. We showed above that the initial total rate of melt production in the asteroid would have been $\sim 100 \text{ m}^3 \text{ s}^{-1}$; if $\sim 200,000$ extraction regions were active, the melt volume flux through each would have been $\sim 0.00045 \text{ m}^3 \text{ s}^{-1}$, whereas if 2–10 such regions were active it would have been ~ 50 to $\sim 10 \text{ m}^3 \text{ s}^{-1}$. We regard the latter scenario as very much more likely, with the compaction length controlling the organization of the vein system within the asteroid and the longest wavelength controlling the number of major melt extraction sites. We thus expect that in the early stages of melting there will be ~ 5 essentially separate regional networks of veins in an asteroid of the size of the UPB, each draining a melt flux of $\phi_R = \sim 20 \text{ m}^3 \text{ s}^{-1}$ toward the surface.

The timescale for growth of Rayleigh–Taylor instabilities, τ , is given by ([Turcotte and Schubert, 2002](#))

$$\tau = [26.08\zeta]/[g\Delta\rho X] \quad (20)$$

where as before ζ is the bulk viscosity of the partially molten matrix and $\Delta\rho$ is the typical density difference driving the instability. For what is probably an extreme porosity variation, from 0.005 to 0.020, between the interiors of solitary waves and the regions between them, the bulk density

difference would be $\sim 10 \text{ kg m}^{-3}$. Then using $\zeta = 3 \times 10^{18} \text{ Pa s}$ as before, we find that for the largest possible vertical scale, $X = 90 \text{ km}$, τ is $21.7 \times 10^{15} \text{ s} = \sim 58 \text{ Ma}$, whereas for the solitary wave scale $X = \sim 350 \text{ m}$, τ is $\sim 4.5 \times 10^{17} \text{ s} = \sim 15 \text{ Ga}$ (3 times the age of the solar system!). Both of these timescales are so much longer than the $\sim 5 \text{ Ma}$ duration of melting ([Fig. 9](#)) that clearly neither large-scale nor small-scale convection of the melting region ever developed to a significant extent. Furthermore, if we substitute for $[g \Delta\rho]$ in [Eq. \(20\)](#) a typical pressure gradient within the asteroid due to the high pressures postulated to be present at the onset of melting, say a few tens of MPa acting over a few tens of km, i.e. $\sim 10^3 \text{ Pa m}^{-1}$, we find relaxation times of 0.03 and 7.4 Ma. These are to be compared with the times needed to achieve pressures of a few tens of MPa, which [Table 2](#) shows to require $\sim 0.2\%$ melting. [Fig. 9](#) shows that 0.2% melting is reached at all depths at about 0.015 Ma after melting starts. Again the timescales for relaxation are greater than the timescale for generation of the relevant stresses (albeit only by a factor of 2 in the case of the larger length scale), thus justifying our earlier assertion that pressures of a few tens of MPa are indeed generated for a short time at the onset of silicate melting and are available to drive the initial crack and vein interconnection processes.

4.5. Melt extraction

The final stage in the evolution of each regional vein network must be the formation of at least one giant vein, which will have the geometry of a planar dike. This is likely to be several km long if it is transferring melt into one of the crustal sills and must be at least ~ 10 km long if it avoids intersecting a sill and instead transfers melt directly to the surface through the permanently cold outer shell of the asteroid. The dike could be up to ~ 40 km long, since this is the depth of the region down to the $\sim 10 \text{ MPa}$ pressure level from which we have meteorites, but to obtain a conservative estimate of the melt transit time we use the minimum value, 10 km, as our upper dike length limit, Y_{max} , showing later that the exact value adopted is not critical. We postulate that the vein network evolves into a fractal-like structure, so that everywhere within the region where melting is taking place a hierarchy of vein lengths exists between the largest and the smallest, which we showed earlier should have a length $Y_{\text{min}} = 1 \text{ mm}$. Melt migrates along a given-sized vein or veins until it encounters the next largest size of vein into which it is driven by either buoyancy or the pressure differential due to the difference in size. Pressure differentials due to vein size differences will relax quickly once a continuously flowing melt network is established, and so we assume, again conservatively, that only melt buoyancy is involved in driving the motion. The density difference, $\Delta\rho$, providing the buoyancy will be the difference between the melt density and the bulk asteroid density, $\sigma = 3300 \text{ kg m}^{-3}$. If smelting is not occurring, the melt density will be $\rho_1 = \sim 2900 \text{ kg m}^{-3}$ and so $\Delta\rho$ will be $\sim 400 \text{ kg m}^{-3}$; we saw earlier that if smelting is taking place the melt will contain $\sim 83\%$ to more than 90% by volume gas bubbles and up to $\sim 30\%$ by mass liquid iron metal droplets, making the bulk density in the range ~ 100 –

300 kg m⁻³ so that $\Delta\rho$ is $\sim 3000\text{--}3200$ kg m⁻³. The melt flow speed through a vein, u_m , is obtained by balancing the buoyancy force against wall friction drag. The standard fluid dynamic relationship for a Newtonian liquid flowing through a circular tube of diameter Z is

$$u_m = (g\Delta\rho Z^2)/(32\eta) \quad (21)$$

if the melt motion in the vein is laminar, which we find to be the case for all permutations of the parameters relevant here.

To determine the equilibrium conditions for melt extraction from the vein network, we assume that there are M classes of vein in the length range between Y_{\max} and Y_{\min} , the veins in each class being longer than the veins in the class beneath it by the factor $(Y_{\max}/Y_{\min})^{(M-1)}$. Melting takes place throughout the asteroid from the center to a radius R_m which, given the ~ 10 km thickness of the cold outer shell, is ~ 90 km. Consider the melt originating at any radial distance R_x from the center of the asteroid and being collected into one of the regional vein networks. Since the total flux through the regional network is ϕ_R , the flux passing through this radius is ϕ_x where

$$\phi_x = (R_x/R_m)^3 \phi_R \quad (22)$$

However, the flux can also be defined as the product of the number N_x of veins cutting through the radius R_x , the area A_x of each vein, $(\pi Z^2)/4$, and the flow speed of melt in the vein, u_m . The number of veins can be found by noting that veins occupy the edges of cubes of length Y_{\min} . Each cube cross-section contains 4 veins, but each vein is shared with 3 adjacent cubes, so that on average there is one vein per cube. The number of cubes of cross-sectional area Y_{\min}^2 intersected by the spherical surface of radius R_x is N_x where

$$N_x = (4\pi R_x^2)/Y_{\min}^2 \quad (23)$$

and so we have

$$(R_x/R_m)^3 \phi_R = [(4\pi R_x^2)/Y_{\min}^2][(\pi Z^2)/4]u_m \quad (24)$$

Substituting for u_m from Eq. (21) and rearranging, the typical vein diameter is given by

$$Z = [(32R_x\phi_R Y_{\min}^2\eta)/(\pi^2 g\Delta\rho R_m^3)]^{1/4} \quad (25)$$

and substituting this expression into Eq. (21) we find the melt speed to be

$$u_m = [(g\Delta\rho R_x\phi_R Y_{\min}^2)/(\pi^2 R_m^3\eta)]^{1/2} \quad (26)$$

Melt flows through veins with diameter Z at this speed until it intersects one of the next largest size of veins in the hierarchy. This larger vein has a length $(Y_{\max}/Y_{\min})^{(M-1)}$ times larger than Y_{\min} , and since we are assuming that these veins are separated by distances equal to their lengths, the time taken by the melt to reach the larger vein is τ where

$$\tau = (3/2)(Y_{\max}/Y_{\min})^{(M-1)}[(32\pi^2 R_m^3\eta)/(g\Delta\rho R_x\phi_R)]^{1/2} \quad (27)$$

The factor $(3/2)$ here allows for the fact that melt in general has to travel laterally as well as vertically to reach the next largest vein. Note that this timescale depends on the ratio $(Y_{\max}/Y_{\min})^{(M-1)}$ but not on the explicit value of the vein length involved. Thus when we consider the melt in this larger vein draining into the next largest vein, the timescale for this step will be essentially the same. As melt moves into ever larger veins there will be an adjustment due to the fact that the melt will be moving closer to the surface of the asteroid and so both the radial distance from the center, R_x , and the acceleration due to gravity, g , will progressively increase, slightly decreasing the transit time. However, since the total melt transit time is the sum of the times involved in each of the M steps this is a relatively small effect.

Table 3 shows examples of the pattern of melt migration for two values of the length multiplication factor

Table 3

Examples of distribution of melt flow properties in interconnected tubular vein network in asteroid. Values follow shortest path through successively larger veins for two values of the length multiplication factor, the factor by which the vein length increases from each class to the next.

Tubular vein length	Distance to asteroid center (km)	Acceleration due to gravity (m s ⁻²)	Tubular vein diameter	Melt flow speed	Reynolds number of melt	Melt transit time	Melt volume fraction
<i>(a) Number of tube size classes = 3, length multiplication factor = 3162</i>							
1.0 mm	52.0	0.0508	73 μ m	26 nm/s	5.7×10^{-9}	5.7 years	6.9×10^{-3}
3.16 m	52.0	0.0509	4.1 mm	83 μ m/s	1.0×10^{-3}	5.7 years	2.2×10^{-6}
10.0 km	62.0	0.0606	0.23 m	0.31 m/s	216	0.62 days	6.9×10^{-10}
Total melt transit time = 12 years							
<i>(b) number of tube size classes = 10, length multiplication factor = 5.995</i>							
1.00 mm	52.0	0.0508	73 μ m	26 nm/s	5.7×10^{-9}	3.9 days	1.2×10^{-2}
5.99 mm	52.0	0.0508	179 μ m	158 nm/s	8.4×10^{-8}	3.9 days	2.1×10^{-3}
3.59 cm	52.0	0.0508	438 μ m	943 nm/s	1.2×10^{-6}	3.9 days	3.5×10^{-4}
0.22 m	52.0	0.0508	1.07 mm	5.6 μ m/s	1.8×10^{-5}	3.9 days	5.8×10^{-5}
1.29 m	52.0	0.0509	2.62 mm	34 μ m/s	2.6×10^{-4}	3.9 days	9.7×10^{-6}
7.74 m	52.0	0.0509	6.43 mm	203 μ m/s	3.9×10^{-3}	3.9 days	1.6×10^{-6}
46.4 m	52.1	0.0509	15.7 mm	1.22 mm/s	5.7×10^{-2}	3.9 days	2.7×10^{-7}
278 m	52.3	0.0512	38.5 mm	7.35 mm/s	0.84	3.9 days	4.5×10^{-8}
1.67 km	54.0	0.0528	94.3 mm	4.55 cm/s	12.8	3.8 days	7.5×10^{-9}
10.0 km	64.0	0.0626	0.23 m	0.31 m/s	223	0.41 days	1.3×10^{-9}
Total melt transit time = 35.4 days							

$(Y_{\max}/Y_{\min})^{(M-1)}$ for the cases where $M = 3$ and $M = 10$. In the $M = 3$ case there are only 2 intermediate sizes of vein between the smallest and largest, whereas in the $M = 10$ case there are 9 progressively increasing sizes. Table 4 shows how the transit time varies with M over a wide range: the minimum melt extraction time occurs between $M = 16$ and 17 with a length multiplication factor of ~ 2.8 . Clearly, melt extraction times will be very long if there are only a few classes in the vein hierarchy, so that melt travels most of the way to the base of the crust through the narrowest veins, but for any value of M greater than ~ 7 , i.e. for length multiplication factors less than ~ 10 – 15 , the typical melt extraction time through the vein network will be just less than 1 month. The volume fraction of the asteroid interior occupied by melt at any one time is given by the sum of the component volume fractions in the last column of Table 3 and is close to 2%. We stress that the above timescales relate to melt extraction early in the melting process, when the total melt production rate is $\sim 100 \text{ m}^3 \text{ s}^{-1}$. Fig. 10 shows that much of the melting takes place at production rates of $\sim 5 \text{ m}^3 \text{ s}^{-1}$, so that with 5 extraction zones the flow rate through each is $\sim 1 \text{ m}^3 \text{ s}^{-1}$. A repeat of all of the above calculations then gives melt transit times of ~ 4 months. The volume fraction of the asteroid interior occupied by melt at any one time during this late stage is then $\sim 0.4\%$. Clearly very nearly all of the melt ever produced in the asteroid interior is extracted to shallow levels.

These melt transit times refer to the time needed for melt to be drained upward out of the zone of melting. We show in the next section that melt is not likely to be erupted directly to the surface but instead is expected to accumulate in a sill near the base of the crust and be erupted episodically to the surface. Thus, technically speaking, transit times to the surface may be much longer. We note, however, that residence in the sill does not need to be included in estimates of the time that the melt was in contact with the mantle residues (hence available for isotopic and geochemical exchange with the residues), and thus does not change the conclusions of Goodrich et al. (2007).

Table 4

Values of the time needed for melt to travel through the vein network within the asteroid as a function of the number of vein length classes, M , and the corresponding factor by which the vein length increases between classes.

Number of classes, M	Vein length scale factor	Melt transit time in veins
2	1×10^7	18,000 years
3	3162	11.5 years
4	215.4	1.14 years
5	56.23	149 days
7	14.68	58.1 days
8	10.00	46.2 days
10	5.995	35.5 days
13	3.831	30.2 days
15	3.162	29.0 days
16	2.929	28.8 days
17	2.738	28.7 days
20	2.336	29.0 days
25	1.957	30.6 days

5. SMELTING AND ITS SIGNIFICANCE FOR THE FATE OF THE MELT

5.1. Explosive volcanism

Next we explore the consequences of smelting for the way in which melt is removed from the asteroid interior and whether it is retained as part of a crust or lost to space. It has previously been suggested (Warren and Kallemeyn, 1992; Scott et al., 1993) that the absence of basaltic urelites can be explained if melts generated on the UPB had high contents of $\text{CO} + \text{CO}_2$ gas derived from smelting, and therefore erupted explosively at velocities sufficient to escape their parent body (Wilson and Keil, 1991). We now reevaluate this conclusion in light of the result (Goodrich et al., 2007) that melting and smelting do not begin simultaneously with one another in all source regions (Fig. 2).

Fig. 3 shows that the onset of smelting, at whatever point it occurs in the course of melting, causes a very large amount of gas to be generated at each pressure level and hence depth. The data in Fig. 3 have been used to evaluate the gas mass fraction, n , and the corresponding gas volume fraction, v , in each 1% increment of smelting at each of the 3, 6.5 and 10 MPa pressure levels. The calculations assume a perfect-gas relationship between pressure and volume, an adequate approximation for the present purpose. It is also assumed that gas and melt are vented to the surface through fractures that form early in the (s)melting process, as discussed below, so that the pressure at all depths remains close to lithostatic. In all cases the gas volume fraction v is greater than 83% at the depth of formation, and is generally greater than 90%; furthermore, the gas volume fraction in a given batch of melt will increase as it decompresses on migrating upward toward lower pressure regions. These values of v are significantly greater than the generally accepted 70–80% threshold in explosive volcanic eruptions for disruption of melt into a spray of liquid droplets transported in the gas phase (Sparks, 1978; Vergnolle and Jaupart, 1988), so it is clear that, as long as no significant net separation of gas and liquid occurs during transport, an issue to which we return later, the release at the surface of melt formed during smelting will be vigorously explosive. The gas mass fraction n can be used to estimate the speed u at which the spray of gas and magma droplets will emerge at the surface in such an eruption using the most conservative of the equations given by Wilson and Keil (1991, 1996):

$$u^2 = [(2nQT)/m][\gamma/(\gamma - 1)] \left\{ 1 - (P_f/P_d)^{[(\gamma-1)/\gamma]} \right\} \quad (28)$$

where $m = 28 \text{ kg kmol}^{-1}$ is the molecular mass of the dominant volatile component, CO (Goodrich et al., 2007); T is the melt temperature in the range 1323–1553 K (Fig. 2); Q is the universal gas constant, $8.314 \text{ kJ K}^{-1} \text{ kmol}^{-1}$; γ is the ratio of the specific heats of the gas, very close to 1.30; and P_f/P_d is the ratio of the final pressure in the expanding gas to the pressure at which disruption of the melt into a spray of droplets takes place. In practice, P_f/P_d is several orders of magnitude less than unity and can be neglected, resulting in the eruption speeds given in Fig. 13. Even though initially high values decline, due to the decline in gas produc-

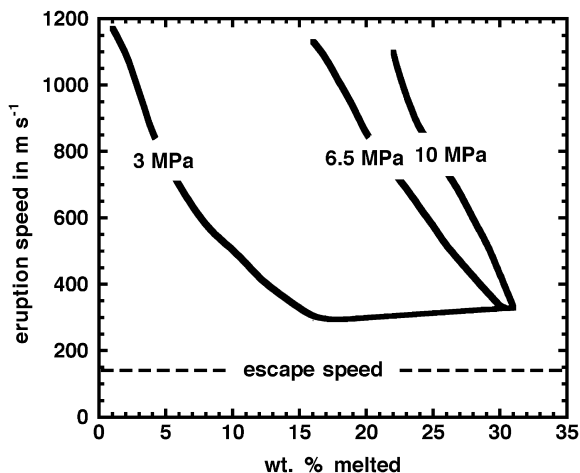


Fig. 13. The speeds at which melts would be erupted at the surface from each of the 3, 6.5 and 10 MPa pressure levels in the UPB as a function of the amount of partial melting that has taken place, during the period in which smelting is taking place. In all cases the speed greatly exceeds the escape velocity.

tion at all levels (Fig. 3), all obtained values are greater than $\sim 300 \text{ m s}^{-1}$. These can be compared with the escape speed, E , from the asteroid given by

$$E = [(8/3)\pi G\sigma]^{1/2}R \quad (29)$$

Using $R = 100 \text{ km}$ and $\sigma = 3300 \text{ kg m}^{-3}$ as before, $E = 136 \text{ m s}^{-1}$, so clearly all of the melt reaching the surface directly during the smelting phase at each depth in the asteroid should be lost to space, rather than being retained on (or beneath) the surface. Thus, our results support the suggestion (Warren and Kallemeyn, 1992; Scott et al., 1993) that explosive volcanism may largely explain the absence of basaltic ureilites in the meteorite collection. However, we now must now consider the consequences of melts produced during the non-smelting phase.

5.2. Mixing of melts during ascent

Goodrich et al. (2007) recognized that a significant fraction of melts generated on the UPB, particularly those from deeper source regions, were produced during periods in which their source regions were not being smelted (Fig. 2 and 3), and suggested that these may have erupted to form a thin crust (estimated 3.3 km thick). However, in that analysis, we overlooked the likelihood that melts derived from all depths would be mixed as they rose. Thus, if gas production is taking place somewhere in the asteroid at all times once melting begins (as one might initially assume from Figs. 2 and 3), then no melt reaching the surface should be gas-free. In fact, this is not quite the case: Fig. 4 shows that, although a given temperature is reached at nearly the same time at all depths greater than $\sim 8 \text{ km}$, there is, nevertheless, a small temperature gradient, such that melting starts first at the deeper levels and is progressively delayed at the shallower levels. The temperature difference between the 6.5 and 10 MPa levels is very much less than that between the 3 and 6.5 MPa levels and so we use the

latter in the following calculation. When the temperature at the 3 MPa level reaches 1323 K, the temperatures at the 6.5 and 10 MPa levels are very close to 1336 K, higher by 13 K. Fig. 2 then implies that about 2.5% melting will have occurred at the 6.5 MPa level and $\sim 1.1\%$ melting will have occurred at the 10 MPa level, in each case with no smelting having taken place. These melts will have been able to rise through their unmelted host rocks as a result of their buoyancy alone, without the added buoyancy provided by accompanying gas bubbles. However, that absence of gas means that, as they pass through the $\sim 8 \text{ km}$ depth level where the temperature decreases rapidly and they encounter first thermally less-altered crust and eventually primitive crust, still containing ice, and probably extensively fractured as a result of the net expansion of the interior of the asteroid caused by the temperature rise during silicate melting. The melts are thus very likely to reach a density trap where they are neutrally buoyant, the conditions being similar to those that appear to have led to volcanic intrusions into the bases of the fractured breccia zones beneath some impact crater floors on the Moon (Wichman and Schultz, 1995). The excess pressure at the upper tip of a column of buoyant melt is given by the integral of the density difference between the melt and its host rocks multiplied by the local acceleration due to gravity, given as a function of depth by Eq. (3). Evaluating this for the likely difference between the densities of the host rocks (3300 kg m^{-3}) and the mafic melt (taken as 2900 kg m^{-3}) yields an excess pressure of at most $\sim 2.5 \text{ MPa}$. This will probably be less than the tensile strength of the crust, which would be $\sim 10 \text{ MPa}$ (Jaeger and Cook, 1979; Ingraffia, 1987) for coherent rock, and somewhat smaller if the pore spaces in the crust were largely filled with cold ice. Thus these early gas-free melts are far more likely to be intruded, either as dikes or sills, somewhere within the outer several km of the crust than to be erupted at the surface.

To estimate the volume of these early intrusions we utilize the volumes of the spherical regions representing the various pressure levels defined in Section 3. Adding 2.5% of the $10.92 \times 10^5 \text{ km}^3$ volume of the 6.5 MPa spherical shell to 1.1% of the $9.82 \times 10^5 \text{ km}^3$ volume of the 10 MPa spherical shell we find a total intruded volume of $38,100 \text{ km}^3$, which is $\sim 3.8\%$ of the total melt volume (almost exactly $1 \times 10^6 \text{ km}^3$) produced over the entire 0–30% melting range. If this volume were intruded uniformly at a depth of, say, 7 km, it would form a global sill 350 m thick. However, as we showed in Section 4.4, the internal structure of the asteroid is likely to evolve to produce a relatively small number (~ 5) of focused volcanic centers. We therefore expect that this same number of early intrusions will form, each containing $\sim 7000\text{--}8000 \text{ km}^3$ of melt. We address their subsequent evolution below.

Once this short initial stage is over, however, it does become the case that gas production is taking place somewhere in the asteroid at all times (i.e. at the 3 MPa level it begins simultaneously with melting at $\sim 1323 \text{ K}$, even though at deeper levels it is delayed). Thus, for the bulk of the asteroid's melting history, when the remaining 96.2% of the total melt is being produced, melts from deep parts of the asteroid where gas production has not yet

started would be expected to mix, as they rise, with gas-containing melts being produced in shallower parts of the body. The calculations underlying Figs. 2 and 3 allow us to find the fraction of the melt from each pressure level that is produced before smelting starts during this period. Multiplying each of these fractions by the volume of the zone centered on the appropriate pressure level from which it comes yields the amount of melt produced without smelting. The values found are 10% of the $2.83 \times 10^5 \text{ km}^3$ of melt from the $9.80 \times 10^5 \text{ km}^3$ volume of the 3 MPa zone, 53% of the $3.15 \times 10^5 \text{ km}^3$ of melt from the $10.92 \times 10^5 \text{ km}^3$ volume of the 6.5 MPa zone, 79% of the $2.83 \times 10^5 \text{ km}^3$ of melt from the $9.82 \times 10^5 \text{ km}^3$ volume of the 10 MPa zone, and 100% of the $0.91 \times 10^5 \text{ km}^3$ of melt from the $3.15 \times 10^5 \text{ km}^3$ volume of the central zone. Thus the total volume of melt produced without smelting during this phase is $\sim 5.1 \times 10^5 \text{ km}^3$. The thermal calculations of Section 3 showed that 15% of this melt, $\sim 0.77 \times 10^5 \text{ km}^3$, was retained in the sill intrusions, the rest being lost into space. The mixing of this retained melt with the $0.38 \times 10^5 \text{ km}^3$ volume of melt intruded into the sill before any smelting started in the asteroid yields a total of $1.15 \times 10^5 \text{ km}^3$. Since the total volume of sill magma was $\sim 1.52 \times 10^5 \text{ km}^3$, this implies that $\sim 76\%$ of the melt in the sill was derived from source regions in which smelting did not take place. This result is consistent with oxygen isotopic data for feldspathic clasts in polymict ureilites, which show a strong bias toward material derived from deeper, more ferroan source regions (Kita et al., 2004, 2006).

The average gas content of the mixture of melt and gas being produced within the UPB can be found, as a function of the temperature history during melting, by combining the gas and melt production functions at all depths within the asteroid. The temperature-dependent patterns of gas production at the 3, 6.5 and 10 MPa levels (Fig. 3) were used to interpolate the corresponding functions at intermediate pressure levels at 1 MPa intervals and the masses of melt and gas produced in each 5 K temperature interval were summed separately. The ratio of these summed masses gives the mean gas content of melt reaching the surface, and Fig. 14 shows the result. The production functions of both the melt and the CO gas depend non-linearly on temperature, and this is reflected in the very non-uniform variation of mean gas content with temperature, and hence with time, values varying between extremes of 15 and 35 wt% over much of the melting temperature range.

This generally large mass fraction of gas in the rising melt has fundamental consequences for the way the two components, gas and liquid, interact as they rise toward the surface through the network of interconnected veins that develops in the interior of the asteroid to feed dikes penetrating through the unmelted crust to the surface. The relatively low pressures in the asteroid interior mean that the gas occupies a large fraction of the volume of the vein and dike network. In volcanic systems on planets as large as Mars, Venus and Earth, the pressures are such that, except very near the surface, exsolved gases form bubbles distributed relatively uniformly throughout the liquid; the gas volume fraction is much less than the 70–90% range over which foams of bubbles distributed in liquids become

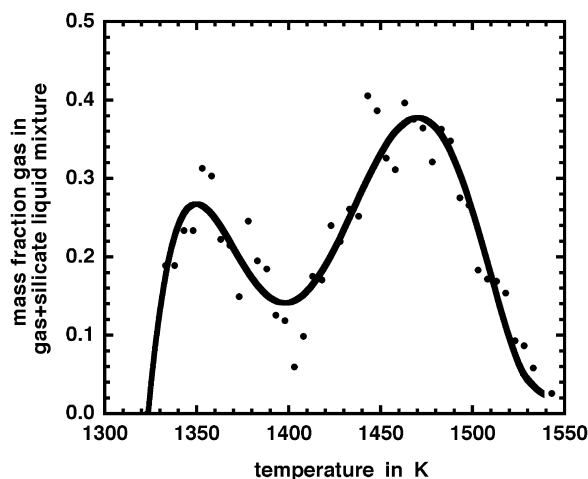


Fig. 14. The variation of the proportion of gas in the mixture of melts and gas from all levels within the UPB as a function of increasing temperature as melting progresses up to 30%. The scatter of points reflects all of the accumulated errors in the methods used to calculate the amounts of liquid and gas produced in the asteroid.

unstable (Jaupart and Vergnolle, 1989). In contrast, the gas volume fraction represented by 15 and 35 wt% of gas in a melt at pressures in the range 3–10 MPa is readily shown, by evaluating the gas volume using the perfect gas law, to range between 0.95 and more than 0.99. Thus foam stability is violated at essentially all depths, and the fluid cannot flow as a uniform dispersion of bubbles distributed throughout the liquid; the mode of transport of the fluid in veins and dikes in the UPB must consist of some kind of two-phase flow (Wallis, 1969). The basic options are either slug flow, in which a series of long, closely-spaced gas bubbles, each nearly as wide as the available pathway, move upward inside a thin film of liquid that slides up the wall, or annular flow, in which a continuous central gas stream replaces the slugs. Intermediates between the various phases exist (Wallis, 1969), and in the case of the UPB, where new gas bubbles are constantly being created by smelting, pure slug flow is impossible – instead bubbly slug flow, in which the liquid surrounding the slugs still contains some gas bubbles, is required. Similarly pure annular flow is unlikely, because the formation, shearing and rupturing of newly formed bubbles will make the interface between the gas core and the liquid film on the walls unstable, and the drop-annular, or annular mist, flow mode, in which liquid droplets are entrained in the gas core, is more likely. In the deep interior, where Section 4.3 shows that the mean vein size is very small, surface tension effects should ensure that liquid films will intermittently break the continuity of the central gas stream if any trend toward annular flow occurs, and so the transport mode will be bubbly slug flow.

However, in the largest veins and pathways into which melt is focused, the flow mode is much more likely to be annular flow. This is particularly true of the final path to the surface in a dike breaching the cold unaltered crust. We have already shown that the small amount of gas-free melt generated in the deep parts of the asteroid before

smelting starts at shallow levels is expected to generate intrusions at the base of the crust. When gas-containing melts are produced, first by the mingling of melts from smelted and non-smelted source regions and subsequently by the mingling of melts from smelted sources at all levels, they will initially be injected into these intrusions. These melts will have a low bulk density, because of the presence of the gas they contain, and so the excess pressure they exert on the existing intruded magma will be larger than that exerted by the early gas-free melts. The integration of the buoyancy due to the density difference between host and melt shows that as the gas content of the melt increases from a low value to $\sim 20\%$ by mass, the excess pressure increases rapidly to a value of ~ 12 MPa and then more slowly to a maximum of ~ 15 MPa. This increase in pressure alone may be enough to fracture the crust above the intrusion allowing eruptions to the surface to begin, the high magma volatile contents ensuring that the eruption speeds exceed the escape velocity (Fig. 13). This is particularly true during the later stages of activity on the asteroid, for every eruption is likely to involve the emplacement of a new dike, and by the end of the eruption some melt will have chilled against the wall of the dike, preventing it from closing completely. This process will progressively add small volumes to the crust, eventually inducing a stress state of horizontal compression that must be overcome to allow a new dike to propagate. If the excess pressure due to magma buoyancy alone is not enough to initiate a dike, a further increase in pressure will occur as additional magma and gas are injected into the intrusion, and an eruption will begin eventually. However, the interval between eruptions will be increased by this requirement for more magma accumulation between events.

Any one eruptive episode is not likely to last long. We showed in Section 3 that in the early stages of melt generation, when the production rate is a maximum, the total for the whole of the UPB is $\sim 100 \text{ m}^3 \text{ s}^{-1}$. If this is divided equally between the suggested 5 volcanic centers the flux reaching each is $\sim 20 \text{ m}^3 \text{ s}^{-1}$. The geometry of the dike needed to accommodate this magma flux reaching the surface can be found using a model of the formation of a dike driven only by magma buoyancy in a brittle, elastic medium developed by Lister and Kerr (1991). Eq. (36) through (39) in Lister and Kerr (1991) give the horizontal dike length, the maximum dike width, and the mean magma flow speed as a function of the vertical extent of the growing dike for given values of the total melt volume flux and the elastic parameters of the host rocks. These equations were implemented as a spreadsheet program and show that in the present case a horizontal length of ~ 7 km and a mean width of ~ 4 cm are required. Table 5 shows some melt transit times for a range of likely vertical lengths of this dike: at mean magma flow speeds of $3\text{--}4 \text{ cm s}^{-1}$ they are of order one week. The fact that the fluid flow mode is likely to involve the annular configuration means that the liquid speed will be somewhat slower than this value, but even at the speed of $3\text{--}4 \text{ cm s}^{-1}$, there will be a problem with the thermal stability of the dike. The transit time from an intrusion at the base of the ~ 10 km thick crust to the surface at 4 cm s^{-1} is $t = 2.5 \times 10^5 \text{ s}$ (~ 70 h). During this time interval a thermal

Table 5

Flow conditions in the final dike that transfers melt from a regional vein network within the asteroid through the cold crust to the surface as a function of the vertical extent of the dike.

Vertical extent (km)	Horizontal extent (km)	Mean width (cm)	Mean melt flow speed (mm s^{-1})	Melt transit time (days)
10	6.7	4.0	38	3.1
15	7.6	3.8	35	5.0
20	8.2	3.7	33	7.1

wave of cooling can travel a distance $\sim (\kappa t)^{1/2}$ where $\kappa = 7 \times 10^{-7} \text{ m}^2 \text{ s}^{-1}$ is the thermal diffusivity of the magma, i.e. ~ 0.4 m or 10 times the 4 cm dike width. Thus excessive cooling is likely to shut off an eruption soon after it starts. The implication is that eruptions are very intermittent rather than continuous (as is, of course, the case on larger planetary bodies). The most likely scenario is that gas-rich magma will be injected into each intrusion between eruptions, increasing the pressure but also allowing time for the gas delivered with the melt to migrate up, as a series of large bubbles as the annular flow encounters the body of melt already in the intrusion, to the top of the intrusion. There the gas will accumulate as a continuous gas pocket overlying a foam of bubbly magma, in turn overlying gas-free magma. When the next fracture to the surface opens, first gas alone will pass through it and then gas and melt will stream out in an extremely gas-rich drop-annular or annular mist flow. The speed of sound in such gas-droplet mixtures is low (Kieffer, 1977), and so the conditions at the surface vent are likely to be choked unless the eruption continues long enough for a considerable amount of erosional widening of the surface vent to occur. As long as the flow is choked, the pressure decrease by the time the intimate gas-droplet mixture reaches the surface will not be large, and so the amount of adiabatic cooling of the mixture will be small. Most of the decompression of the gas phase and the acceleration and cooling of the gas-droplet mixture, with eventual freezing of the droplets, will then occur (e.g. Kieffer, 1989) through a series of shocks above the vent. The very high final eruption speed will ensure that the frozen melt droplets are accelerated to much greater than escape velocity and leave the asteroid. However, this process of concentration of gas into the upper part of the intrusion during the repose periods between eruptions will ensure that on average some fraction of the melt entering the intrusion is retained within it, progressively increasing its volume.

The ratio of the retained to erupted magma volumes in any one recharge-eruption cycle can be estimated as follows. Magma flows into the intrusion with a gas content that ranges up to $\sim 35\%$ by mass (Fig. 14). The gas will be distributed in the melt as a mixture of small, recently-generated gas bubbles and larger bubbles representing the slugs present in the larger veins draining the interior. The pressure in the incoming magma will be relatively low immediately after an eruption because most of the excess pressure generated by magma buoyancy will be expended against driving the magma motion. However, as the

intrusion inflates, the inflow speed will decrease and the pressure will rise toward the $\sim 12\text{--}15$ MPa level consistent with the magma buoyancy. At some point the crust overlying the intrusion fails and an eruption starts. Magma initially flows to the surface at a rate consistent with the excess pressure in the reservoir; as this pressure decreases the buoyancy of the melt-gas mixture takes over control of the eruption rate. The gas bubbles in the melt expand as the pressure in the reservoir decreases and continue to do so, driving out both gas and melt, until either the pressure in the intrusion decreases to the ambient lithostatic load, ~ 1 MPa at the roof of the intrusion, or the gas bubble volume fraction in the melt reaches the critical value at which the foam collapses and gas escapes without further significant liquid loss. If the critical bubble volume fraction for foam collapse is f_c and gas mass fraction is n , it is readily shown that the fraction of the melt that is retained at the end of an eruptive event, m_r , is equal to $[(1 - f_c)/(1 - n)]$. Fig. 15 shows the variation of m_r with n for three values of f_c covering the 0.7–0.9 range generally judged to be relevant to magmatic foams (Jaupart and Vergnolle, 1989). With an uncertainty of about a factor of 2, we expect that $\sim 25\%$ of all of the melt from the interior of the asteroid will be retained in the crustal intrusions, a total volume of $\sim 253,000$ km³. This result may be compared with the finding from the thermal modeling of the asteroid interior described in Section 3 where it was estimated that $\sim 15\%$ of the melt was retained in the intrusion. The estimates from these two approaches would agree exactly if the critical bubble volume fraction for foam collapse were 0.9, at the upper end of the likely range.

5.3. Loss of asteroid mass due to explosive volcanism

We now address the concern raised by Warren and Huber (2006) that the loss of asteroid mass due to explosive

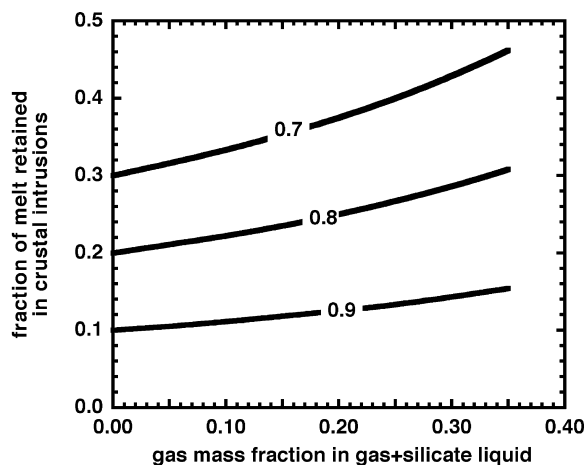


Fig. 15. The fraction of all of the melt produced in the UPB that is retained as shallow intrusions in the crust rather than being erupted explosively into space. Eruptions occur when fresh melt and gas are injected at the base of the intrusion and mix with melt currently in the intrusion to produce an unstable foam. The curves correspond to assuming that collapse of the gas–liquid foam takes place when the volume fraction of gas bubbles reaches 0.7, 0.8 or 0.9.

volcanism on the UPB would have led to a diminution in pressure that would have caused a runaway smelting process (although there is no evidence for this in ureilites). If 75% of the melt is lost through explosive eruptions in the way described in the previous section, this corresponds to $\sim 17\%$ of the asteroid volume, which produces a reduction in its radius from 100 to ~ 94 km. This $\sim 6\%$ change in body radius due to the loss of the explosively erupted melt has the effect of reducing the pressure at any given depth by between 6% and 8% by the end of the melting/smelting process. This would imply, for example, that in the material originally at the depth corresponding to 6.5 MPa pressure, smelting would begin at $\sim 14.8\%$ melting instead of at $\sim 16\%$ melting, and that material originally at the 10 MPa level would start smelting after $\sim 21.3\%$ melting instead of $\sim 22.1\%$ melting. Thus, our results do not support the assertion of Warren and Huber (2006) that the loss of asteroid mass due to explosive volcanism on the UPB would have caused a runaway smelting process.

We note that the above conclusions about a fraction of the melts being retained as intrusions depend on their not containing significant amounts of carbon, because if they did they would be progressively smelted during ascent. Goodrich et al. (2007) calculated the amounts of gas that would be generated by smelting during isothermal ($T = 1050\text{--}1250$ °C) ascent of carbon-bearing melts on the UPB (see Fig. 12 of that paper) and found that they would be substantial, ranging up to 11 wt%. Equating the escape speed E from Eq. (4) to the explosive eruption speed u from Eq. (4) and solving for the gas content n that just allows escape speed to be reached, we find that all gas contents greater than 0.6 wt% lead to explosive loss of the melts – thus it is impossible that these melts would have been retained. In addition, if all melts were smelted in this way during ascent on the UPB, they would have become highly magnesian. This prediction is in contrast to what is observed in polymict ureilites. The most abundant indigenous feldspathic melt lithologies that have been identified in polymict ureilites (i.e. melt material that was not lost) are notably more ferroan than main group ureilites, and show normal (i.e. not carbon-redox-controlled) fractionation trends (Ikeda et al., 2000; Cohen et al., 2004; Goodrich et al., 2004). Thus, we emphasize the distinction between melts produced from source regions that are being smelted and smelted melts. The former do not necessarily become the latter, unless they carry carbon with them or react with carbon in shallower regions. Considering the low density of graphite, it might seem likely to be carried upward in the melts; however, it is possible that the size of the graphite grains in the source regions precluded their being transported in initial melt conduits. We showed in Section 4.3 that much of the interconnected network through which melt must migrate involves veins no wider than ~ 30 microns, and the size of inferred primary graphite grains in low-shock ureilites is much larger than this (Berkley and Jones, 1982; Treiman and Berkley, 1994). Thus physical transport is unlikely. Transport by solution is also unlikely because of the very low solubility of elemental carbon in basaltic melts at the pressures relevant here (e.g. Pawley et al., 1992). With regard to possible interactions with car-

bon in shallower regions, the rapidity with which the melts rise would preclude any reaction during ascent, and the volume of the sill would likely preclude reaction on any substantial scale (except to a limited degree along the contacts with surrounding rock). Thus, we conclude that, regardless of whether they were derived from source regions that were being smelted or source regions that were not being smelted, the majority of melts produced on the UPB were not themselves smelted.

5.4. The sill and the origin of feldspathic clasts in polymict ureilites

We now return to the issue of the geometry of the crustal intrusions and show how this is linked to ^{26}Al – ^{26}Mg , ^{53}Mn – ^{53}Cr and Pb–Pb data giving ages of ~ 5 Ma after CAI for feldspathic clasts in polymict ureilites (Goodrich et al., 2002a; Kita et al., 2002, 2003, 2007). At first glance, the results of our thermal modeling (Section 3) appear to be grossly inconsistent with these data, since they clearly show that any reasonably plagioclase-saturated (i.e. “basaltic”) melts on the UPB must have been generated much earlier, at ~ 0.9 – 1 Ma after CAI (Fig. 9). We suggest that this problem is resolved if the feldspathic clasts represent basaltic melts that were stored for ~ 4 Ma, cooling slowly until they reach isotopic closure (a temperature somewhat less than 700°C , say 950K), in crustal intrusions (i.e. the sill).

We now show that the likely geometry of the intrusions is consistent with this interpretation. Section 5.2 showed that we expect $\sim 253,000\text{ km}^3$ of intruded magma to be accumulated in intrusions in the crust. If all of this volume were distributed uniformly around the asteroid at ~ 7 km depth it would form a global sill ~ 2.3 km thick. However, we showed in Section 4.4 that the internal structure of the asteroid is likely to evolve to produce a relatively small number (~ 5) of focused volcanic centers. If a similar number of intrusions forms, each one is likely to evolve into a much more equant shape, as is the case for shallow magma reservoirs in volcanic areas on Earth and Mars. If the total intruded magma volume were distributed equally among 5 magma reservoirs, each would have a volume V_r of $50,600\text{ km}^3$. Assume that the shape of each is that of an oblate ellipsoid, with horizontal axes of length X_r and a vertical extent Z_r ; then $V_r = (\pi/6) X_r^2 Z_r$. We can constrain the value of Z_r by noting that the supply rate of magma is large (Fig. 10) for a period that is short compared with the decay constant of ^{26}Al and then declines rapidly. This implies that the magma reservoir is constructed quickly and then survives in a way that balances conductive heat losses into its surroundings against ongoing heat generation by ^{26}Al decay. If the heat production rate in W m^{-3} at the time of formation is H_0 , then after the reservoir has been present for time t_i the total heat production rate is $H_0(\pi/6)X_r^2 Z_r \exp(-t_i/\tau)$ Watts. The reservoir mainly loses heat by conduction upward to the surface through the cylindrical region above it which has a horizontal area equal to that of the reservoir, $(\pi/4)X_r^2$, and so the heat flow rate per unit surface area is $[H_0(\pi/6)X_r^2 Z_r \exp(-t_i/\tau)] / [(\pi/4)X_r^2]$, which simplifies to $(2/3)H_0 Z_r \exp(-t_i/\tau)$ Watts per square meter. But this heat flux must be equal to the

heat flow rate determined to the temperature gradient between the reservoir and the surface, equal to $K_c(\theta_r - \theta_s)/D_r$, where K_c is the thermal conductivity of the crust, D_r is the depth of the top of the reservoir, and θ_r and θ_s are the temperatures of the reservoir and surface, respectively. Equating the heat fluxes and solving for Z_r we have

$$Z_r = [3K_c(\theta_r - \theta_s) \exp(t_i/\tau)] / (2D_r H_0) \quad (30)$$

The surface temperature θ_s is assumed fixed at the formation temperature, 250K . Given the temperature range in the crust above the reservoir and the likely presence of residual ice in the shallowest part we take the average thermal conductivity K_c to be $1\text{ W m}^{-1}\text{ K}^{-1}$. It was suggested earlier that the intrusion probably started to form at a depth of ~ 7 km and so we adopt this value for D_r . The reservoir forms in a short time interval at about 1 Ma after CAI; with an initial ^{26}Al activity at CAI time of $2.156 \times 10^{-7}\text{ W kg}^{-1}$, i.e. $7.114 \times 10^{-4}\text{ W m}^{-3}$, and allowing for the enhancement of ^{26}Al in the melt relative to the rest of the asteroid, the value of H_0 is $1.56 \times 10^{-3}\text{ W m}^{-3}$. If we now input the constraint (based on our suggestion) that the reservoir temperature θ_r was 950K at 5 Ma after CAI, i.e. at a time $t_i = 4$ Ma after the reservoir formed, we find a vertical reservoir extent of $Z_r = 4.67\text{ km}$ which, with $V_r = 50,600\text{ km}^3$ implies a horizontal reservoir extent of $X_r = \sim 144\text{ km}$. For comparison, these dimensions are within a factor of 2 of those estimated for many of the reservoirs beneath the summits of the large shield volcanoes on Mars. More importantly, the total plan-view area of 5 intrusions with diameters of 144 km is $\sim 81,000\text{ km}^2$. The area of a spherical shell at a depth of 7 km in a 100 km radius asteroid is $\sim 109,000\text{ km}^2$; thus our putative 5 intrusions very nearly do represent a global sill. While there are numerous uncertainties involved in making these reservoir size estimates, it is clear that plausible geometries are entirely consistent with the hypothesis that the feldspathic clasts in polymict ureilites represent melts that were stored in shallow intrusions, rather than any remnants of melts that erupted explosively from the surface of the body. As discussed above, such a conclusion would also resolve the apparent puzzle that these feldspathic lithologies show normal igneous fractionation trends, rather than carbon redox control, and thus appear to have not been smelted (Cohen et al., 2004; Goodrich et al., 2004).

5.5. The fate of metal on the UPB

As discussed in Goodrich et al. (2007), our model implies that most of the iron metal produced by smelting on the UPB was lost from the meteorites. In that work, we modeled the loss of metal, assumed to be completely liquid, by assuming that the amounts of CO and CO_2 generated by smelting during each increment of silicate melting were distributed evenly between the corresponding amount of metal and silicate melt produced. This calculation led to the conclusion that the bulk density of the metal + gas fluid was such that it would be driven upwards and lost due to explosive volcanism. However, in that treatment, we overlooked the likelihood that the metallic melt and the silicate melt would be immiscible, and as a consequence did not explore

in detail the physical interactions between liquid metal droplets, the host silicate liquid and, where the gas phase forms slugs or annular flow, the interaction between the liquid metal droplets and the gas. As outlined in Section 3, consideration of these details strongly suggests that liquid metal droplets will migrate downward, not upward. We emphasize, however, that these conclusions about the fate of the metal are still preliminary, because the composition of primary metal on the UPB, and therefore the degree to which it was liquid, still require further study.

6. PETROLOGICAL AND GEOCHEMICAL IMPLICATIONS

Some of the results of this work, in preliminary form, were used by Goodrich et al. (2007). In particular, we used the result that melt extraction on the UPB would have been a rapid, near-fractional process to demonstrate that equilibrium partitioning of oxygen isotopes and trace (rare earth) elements between melts and residues (i.e. main group ureilites) would not have been attained. We emphasize that the detailed calculations presented here entirely support that conclusion. We have, however, now shown that melt is not likely to be erupted directly to the surface but instead is expected to accumulate in a shallow intrusion (sill) and be erupted episodically to the surface, a scenario not envisioned in our earlier work. Nevertheless, residence in the sill does not need to be included in estimates of the time that the melt was in contact with the mantle residues (hence available for isotopic and geochemical exchange with the residues), and thus does not change the conclusions of Goodrich et al. (2007).

The likelihood that melts on the UPB would form a shallow intrusion or intrusions is, in fact, one of the most important new results of the present work. Goodrich et al. (2007) suggested that all melts produced during the non-smelting stage in any source region on the UPB might erupt to the surface to form a thin crust. We have now shown (1) that the total volume of gas-poor melt is significantly less than assumed by Goodrich et al. (2007), due to mixing of melts during ascent, and (2) that the gas-poor melts are more likely to be intruded at the base of the cold outer shell of the asteroid (due to a density trap) than to be erupted into flows. The latter conclusion is particularly significant, as it provides an explanation for the ~5 Ma after CAI ages of feldspathic clasts in polymict ureilites. The interpretation that these clasts represent basaltic melts that were generated at ~0.9–1 Ma after CAI and then stored in a sill for ~4 Ma until they reach isotopic closure, differs significantly from previous thermal modeling that attempted to explain the generation of these melts at 5 Ma after CAI (Kita et al., 2005). At the same time, our thermal model successfully produces main group ureilites as the final residues of ~30% melt extraction at all depths (Goodrich et al., 2007) at ~5 Ma after CAI, which is consistent with the U–Pb age of META 78008 (Torigoye-Kita et al., 1995). Again, the sill is essential, as it provides the extra heat required to achieve the requisite high temperatures (hence 30% melting) in the shallowest source regions.

Our results regarding the existence and thermal history of the sill (or shallow intrusions) have important implications for petrologic interpretations of the feldspathic materials in polymict ureilites. Given its long cooling history, the sill would be expected to differentiate, forming evolved melts and cumulates. The most abundant population of feldspathic clasts in polymict ureilites (the “albitic lithology”) shows an extreme degree of fractionation (Ikeda et al., 2000; Goodrich et al., 2002a, 2004; Cohen et al., 2004; Kita et al., 2004), and thus is consistent with this interpretation (in fact, formation of such a highly-evolved lithology in a slowly cooling sill is much more reasonable than formation during an explosive eruption). Some of the unusual mafic clasts in polymict ureilites (e.g. Goodrich and Keil, 2002; Cohen et al., 2004) might, therefore, be cumulates formed in this sill. Most importantly, then, if our interpretation that the feldspathic materials in polymict ureilites are derived from a sill (rather than being remnants of explosively erupted melts) is correct, then none of them may be directly complementary to the ultramafic ureilite residues.

Our model also implies the existence of two other types of materials that might be present in polymict ureilites – “primitive” ureilite precursor material from the cold outer shell, and variously metamorphosed versions of that material from near the contact with the sill. Rare, phyllosilicate-bearing dark clasts that occur in polymict ureilites have been discussed as possible samples of ureilite precursor material (Prinz et al., 1987; Brearley and Prinz, 1992; Ikeda et al., 2000, 2003; Goodrich and Keil, 2002; Goodrich et al., 2004), although it is not clear that their oxygen isotopic compositions are consistent with derivation from the UPB (Brearley and Prinz, 1992). To our knowledge, none of the wide variety of clasts in polymict ureilites have been examined to determine whether they could be “baked” versions of ureilite precursors, but our model suggests that such material might be similar to the anhydrous dark clasts in Allende (e.g. Krot et al., 1997), and should be sought.

ACKNOWLEDGMENTS

We thank Noriko Kita and Hap McSween for helpful discussions, and Tim McCoy, Ed Scott, Norm Sleep and David Mittlefehldt for constructive reviews. This work was supported by NASA Grants NNG05GH72G and NNX08AG63G to C.A. Goodrich, NASA Grant NAG5-11591 to K. Keil, and NSF Grants 0337125 and 0322766 to J.A. Van Orman.

REFERENCES

- Berkley J. L. and Jones J. H. (1982) Primary igneous carbon in ureilites: petrological implications. *Proc. Lunar Planet. Sci. Conf.* **13**, A353–A364.
- Bizzarro M., Joel A., Baker J. A., Haack H. and Lundgaard K. L. (2005) Rapid timescales for accretion and melting of differentiated planetesimals inferred from ^{26}Al – ^{26}Mg chronometry. *Astrophys. J. Lett.* **632**, L41–L44. doi:10.1086/497638.
- Brearley A. J. and Jones R. H. (1998) Chondritic meteorites. In *Planetary Materials*, vol. 36 (ed. J. J. Papike). Mineralogical Society of America. Rev. Mineral., p. 398 pp.

- Breary A. J. and Prinz M. (1992) CI chondrite-like clasts in the Nilpena polymict ureilite. Implications for aqueous alteration processes in CI chondrites. *Geochim. Cosmochim. Acta* **56**, 1373–1386.
- Carlsaw H. S. and Jaeger J. C. (1947) *Conduction of Heat in Solids*. Clarendon Press, Oxford, 386 pp.
- Cohen B. A. and Coker R. F. (2000) Modeling of liquid water on CM meteorite parent bodies and implications for amino acid racemization. *Icarus* **145**, 369–381.
- Cohen B. A., Goodrich C. A. and Keil K. (2004) Feldspathic clast populations in polymict ureilites: stalking the missing basalts from the ureilite parent body. *Geochim. Cosmochim. Acta* **68**, 4249–4266.
- Dobran F. (2001) *Volcanic Process – Mechanisms in Magma Transport*. Kluwer Academic/Plenum Press, New York, 590 pp.
- Downes H., Mittlefehldt D. W., Kita N. T. and Valley J.W. (in press) Evidence from polymict ureilites for a disrupted and re-accreted single ureilite parent asteroid gardened by several distinct impactors. *Geochim. Cosmochim. Acta*.
- Fowler A. C. (1985) A mathematical model of melt transport in the asthenosphere. *Geophys. Astrophys. Fluid Dyn.* **33**, 63–96.
- Goodrich C. A. (1992) Ureilites: a critical review. *Meteoritics* **27**, 327–352.
- Goodrich C. A. (1999) Are ureilites residues from partial melting of chondritic material? The answer from MAGPOX. *Meteorit. Planet. Sci.* **34**, 109–119.
- Goodrich C. A. and Delaney J. S. (2000) Fe/Mg–Fe/Mn relations of meteorites and primary heterogeneity of primitive achondrite parent bodies. *Geochim. Cosmochim. Acta* **64**, 2255–2273.
- Goodrich C. A. and Keil K. (2002) Feldspathic and other unusual clasts in polymict ureilite DaG 165. *Lunar Planet. Sci.* **33**, 1777 (abstr.).
- Goodrich C. A., Jones J. H. and Berkley J. L. (1987) Origin and evolution of the ureilite parent magmas: multi-stage igneous activity on a large parent body. *Geochim. Cosmochim. Acta* **51**, 2255–2273.
- Goodrich C. A., Hutcheon I. D. and Keil K. (2002a) ^{53}Mn – ^{53}Cr age of a highly-evolved, igneous lithology in polymict ureilite DaG 165. *Meteorit. Planet. Sci.* **37**, A54 (abstr.).
- Goodrich C. A., Krot A. N., Scott E. R. D., Fioretti A. M. and Keil K. (2002b) Formation and evolution of the ureilite parent body and its offspring. *Lunar Planet. Sci.* **33**, #1379 (abstr.).
- Goodrich C. A., Scott E. R. D. and Fioretti A. M. (2004) Ureilitic breccias: clues to the petrologic structure and impact disruption of the ureilite parent asteroid. *Chem. Erde* **64**, 283–327.
- Goodrich C. A., Wlotzka F., Ross D. K. and Bartoschewitz R. (2006) Northwest Africa 1500: plagioclase-bearing monomict ureilite or unique achondrite?. *Meteorit. Planet. Sci.* **41** 925–952.
- Goodrich C. A., Van Orman J. and Wilson L. (2007) Fractional melting and smelting on the ureilite parent body. *Geochim. Cosmochim. Acta* **71**, 2876–2895.
- Hart S. R. (1993) Equilibration during mantle melting: a fractal tree model. *Proc. Natl. Acad. Sci. USA* **90**, 11,914–11,918.
- Hevey P. J. and Sanders I. S. (2006) A model for planetesimal meltdown by ^{26}Al and its implications for meteorite parent bodies. *Meteorit. Planet. Sci.* **41**(1), 95–106.
- Ikeda Y. and Prinz M. (2001) Magmatic inclusions and felsic clasts in the Dar al Gani 319 polymict ureilite. *Meteorit. Planet. Sci.* **36**, 481–499.
- Ikeda Y., Prinz M. and Nehru C. E. (2000) Lithic and mineral clasts in the Dar al Gani (DAG) 319 polymict ureilite. *Antarct. Meteorit. Res.* **13**, 177–221.
- Ikeda Y., Kita N. T., Morishita Y. and Weisberg M. K. (2003) Primitive clasts in the Dar al Gani 319 polymict ureilite: precursors of the ureilites. *Antarct. Meteorit. Res.* **16**, 105–127.
- Ingraffia A. R. (1987) Theory of crack initiation and propagation in rock. In *Fracture Mechanics of Rock* (ed. B. K. Atkinson). Academic Press, San Diego, California, pp. 277–349.
- Jaeger J. C. and Cook N. G. W. (1979) *Fundamental of Rock Mechanics*, third ed. Chapman and Hall, New York, 593 pp.
- Jaupart C. and Vergnolle S. (1989) The generation and collapse of a foam layer at the roof of a basaltic magma chamber. *J. Fluid Mech.* **203**, 347–380.
- Keil K. and Wilson L. (1993) Explosive volcanism and the compositions of cores of differentiated asteroids. *Earth Planet. Sci. Lett.* **117**, 111–124.
- Kelemen P. B., Hirth G., Shimizu N., Spiegelman N. and Dick H. J. B. (1997) A review of melt migration processes in the adiabatically upwelling mantle beneath oceanic spreading ridges. *Philos. Trans. R. Soc. A* **355**, 1–35.
- Kieffer S. W. (1977) Sound speed in liquid–gas mixtures: water–air and water–steam. *J. Geophys. Res.* **82**, 2895–2904.
- Kieffer S. W. (1989) Geologic nozzles. *Rev. Geophys.* **27**(1), 3–38.
- Kita N. T., Ikeda Y. and Morishita Y. (2002) The old Pb–Pb age of apatite in felsic clast of polymict ureilite DaG 319. *Meteorit. Planet. Sci.* **37**, A79 (abstr.).
- Kita N. T., Ikeda Y., Shimoda H., Togashi Y. and Morishita S. (2003) Timing of basaltic volcanism in ureilite parent body inferred from the ^{26}Al ages of plagioclase-bearing clasts in DaG 319 polymict ureilite. *Lunar Planet. Sci.* **34**, #1557 (abstr.).
- Kita N. T., Ikeda Y., Togashi S., Liu Y., Morishita Y. and Weisberg M. K. (2004) Origin of ureilites inferred from a SIMS oxygen isotopic and trace element study of clasts in the Dar al Gani 319 polymict ureilite. *Geochim. Cosmochim. Acta* **68**, 4213–4235.
- Kita N. T., Ikeda Y., Shimoda G., Togashi S., Morishita Y. and Weisberg M. K. (2005) Internal heating of the ureilite parent body by short-lived nuclides. *Meteorit. Planet. Sci.* **40**, 5178 (abstr.).
- Kita N. T., Goodrich C. A., Fu B., Spicuzza M. J. and Valley J. W. (2006) Oxygen isotopes in mafic and feldspathic clasts from polymict ureilites. *Meteorit. Planet. Sci.* **41**, A96 (abstr.).
- Kita N. T., Hutcheon I. D., Huss G. and Goodrich C. A. (2007) ^{26}Al – ^{26}Mg and ^{53}Mn – ^{53}Cr age of a feldspathic lithology in polymict ureilites. *Meteorit. Planet. Sci.* **42**(Suppl. 1), A83 (abstr.).
- Krot A. N., Scott E. R. D. and Zolensky M. E. (1997) Origin of fayalitic olivine rims and lath-shaped matrix olivine in the CV3 chondrite Allende and its dark inclusions. *Meteorit. Planet. Sci.* **32**, 31–49.
- Lim L. F., McConnochie T. H., Bell J. F. and Hayward T. L. (2005) Thermal infrared (8–13 μm) spectra of 29 asteroids: the cornell mid-infrared asteroid spectroscopy (MIDAS) survey. *Icarus* **173**(2), 385–408.
- Lister J. R. and Kerr R. C. (1991) Fluid-mechanical models of crack propagation and their application to magma transport in dykes. *J. Geophys. Res.* **96**(B6), 10,049–10,077.
- Maaloe S. (1981) Magma accumulation in the ascending mantle. *J. Geol. Soc. Lond.* **138**, 223–236.
- Maaloe S. (2003) Melt dynamics of a partially molten mantle with randomly oriented veins. *J. Petrol.* **44**, 1193–1210.
- Maaloe S. and Schie A. (1982) The permeability controlled accumulation of primary magma. *Contrib. Mineral. Petrol.* **81**, 350–357.
- McCord T. B. and Sotin C. (2005) Ceres: evolution and current state. *J. Geophys. Res.* **110**, E05009. doi:10.1029/2004JE002244.
- McKenzie D. P. (1984) The generation and compaction of partial molten rock. *J. Petrol.* **25**, 713–765.
- Mittlefehldt D. W. (1986) Fe–Mg–Mn relations of ureilite olivines and pyroxenes and the genesis of ureilites. *Geochim. Cosmochim. Acta* **50**, 107–110.

- Mittlefehldt D. W., McCoy T. J., Goodrich C. A. and Kracher A. (1998) Non-chondritic meteorites from asteroidal bodies. In *Planetary Materials*, vol. 36 (ed. J. J. Papike). 195 pp.
- Mittlefehldt D. W., Hudon P. and Galindo, Jr., C. (2005) Petrology, geochemistry and genesis of ureilites. *Lunar Planet. Sci.* **36**, #1140 (abstr.).
- Muenow D. M., Keil K. and Wilson L. (1992) High-temperature mass spectrometric degassing of enstatite chondrites: implications for pyroclastic volcanism on the aubrite parent body. *Geochim. Cosmochim. Acta* **56**, 4267–4280.
- Nicolas A. (1986) A melt extraction model based on structural studies in mantle peridotites. *J. Petrol.* **27**, 999–1022.
- Nicolas A. and Jackson M. (1982) High temperature dikes in peridotites: origin by hydraulic fracturing. *J. Petrol.* **23**, 568–582.
- Parfitt E. (1991) The role of rift-zone storage in controlling the site and timing of eruptions and intrusions of Kilauea volcano, Hawai'i. *J. Geophys. Res.* **96**, 10101–10112.
- Pawley A. R., Holloway J. R. and McMillan P. F. (1992) The effect of oxygen fugacity on the solubility of carbon–oxygen fluids in basaltic melt. *Earth Planet. Sci. Lett.* **110**, 213–225.
- Prinz M., Weisberg M. K., Nehru C. E. and Delaney J. S. (1987) EET83309, a polymict ureilite: recognition of a new group. *Lunar Planet. Sci.* **18**, 802–803 (abstr.).
- Ribe N. M. (1985) The deformation and compaction of partially molten zones. *Geophys. J. R. Astron. Soc.* **83**, 487–501.
- Richter F. M. and McKenzie D. (1984) Dynamical models for melt extraction from a deformable matrix. *J. Geol.* **92**, 729–740.
- Rubin A. M. (1993) Tensile fracture of rock at high confining pressure: implications for dike propagation. *J. Geophys. Res.* **98**, 15919–15935.
- Sahijpal S., Soni P. and Gupta G. (2007) Numerical simulations of the differentiation of accreting planetesimals with ^{26}Al and ^{60}Fe as the heat sources. *Meteorit. Planet. Sci.* **42**(9), 1529–1548.
- Scott E. R. D., Taylor G. J. and Keil K. (1993) Origin of ureilite meteorites and implications for planetary accretion. *Geophys. Res. Lett.* **20**, 415–418.
- Scott D. R. and Stevenson D. J. (1984) Magma solitons. *Geophys. Res. Lett.* **11**, 1161–1164.
- Scott D. R. and Stevenson D. J. (1986) Magma ascent by porous flow. *J. Geophys. Res.* **91**, 9283–9296.
- Singletary S. J. and Grove T. L. (2003) Early petrologic processes on the ureilite parent body. *Meteorit. Planet. Sci.* **38**, 95–108.
- Sinha S. K., Sack R. O. and Lipschutz M. E. (1997) Ureilite meteorites: equilibration temperatures and smelting reactions. *Geochim. Cosmochim. Acta* **61**, 4242–4325.
- Sleep N. H. (1974) Segregation of magma from a mostly crystalline mush. *Geol. Soc. Am. Bull.* **85**, 1225–1232.
- Sleep N. H. (1984) Tapping of magma from ubiquitous mantle heterogeneities: an alternative to mantle plumes? *J. Geophys. Res.* **89**, 10029–10041.
- Sleep N. H. (1988) Tapping of melt by veins and dikes. *J. Geophys. Res.* **93**, 10255–10272.
- Sparks R. S. J. (1978) The dynamics of bubble formation and growth in magmas: a review and analysis. *J. Volcanol. Geoth. Res.* **3**, 1–37.
- Spence D. A., Sharp P. W. and Turcotte D. L. (1987) Buoyancy-driven crack propagation: a mechanism for magma migration. *J. Fluid Mech.* **184**, 135–153.
- Spiegelman M. and Elliot T. (1993) Consequences of melt transport for uranium series disequilibrium. *Earth Planet. Sci. Lett.* **118**, 1–20.
- Spiegelman M. (1993a) Flow in deformable porous media. Part 1 simple analysis. *J. Fluid Mech.* **247**, 17–38.
- Spiegelman M. (1993b) Flow in deformable porous media. Part 2 numerical analysis – the relationship between shock waves and solitary waves. *J. Fluid Mech.* **247**, 39–63.
- Spiegelman M. and McKenzie D. (1987) Simple 2-D models for melt extraction at mid-ocean ridges and island arcs. *Earth Planet. Sci. Lett.* **83**, 137–152.
- Tait S. R., Jaupart C. and Vergnolle S. (1989) Pressure, gas content and eruptive periodicity of a shallow crystallising magma chamber. *Earth Planet. Sci. Lett.* **92**, 107–123.
- Torigoye-Kita N., Tatsumoto M., Meeker G. P. and Yanai K. (1995) The 4.56 Ga U–Pb age of MET 78008 ureilite. *Geochim. Cosmochim. Acta* **59**, 2319–2329.
- Treiman A. H. and Berkley J. L. (1994) Igneous petrology of the new ureilites Nova 001 and Nullarbor 010. *Meteoritics* **29**, 843–848.
- Turcotte D. L. and Schubert G. (2002) *Geodynamics*. Cambridge University Press, 275 pp.
- Valentini L., Perugini D. and Poli G. (2007) The ‘small-world’ nature of fracture/conduit networks: possible implications for disequilibrium transport of magmas beneath mid-ocean ridges. *J. Volcanol. Geoth. Res.* **159**(4), 355–365.
- Vergnolle S. and Jaupart C. (1988) Laboratory models of Hawaiian and Strombolian eruptions. *Nature* **331**, 58–60.
- von Barga N. and Waff H. S. (1986) Permeabilities, interfacial areas and curvatures of partially molten systems: results of numerical computations of equilibrium microstructures. *J. Geophys. Res.* **91**, 9261–9276.
- Walker D. and Grove T. L. (1993) Ureilite smelting. *Meteoritics* **28**, 629–636.
- Wallis G. B. (1969) *One-Dimensional Two-Phase Flow*. McGraw-Hill, New York, 480 pp.
- Warren P. H. and Huber H. (2006) Ureilite petrogenesis: a limited role for smelting during anatexis and catastrophic disruption. *Meteorit. Planet. Sci.* **41**, 835–849.
- Warren P. H. and Kallemeyn G. W. (1992) Explosive volcanism and the graphite-oxygen fugacity buffer on the parent asteroid(s) of the ureilite meteorites. *Icarus* **100**, 110–126.
- Warren P. H., Ulf-Moeller F., Huber H. and Kallemeyn G. W. (2006) Siderophile geochemistry of ureilites: a record of early stages of planetesimal core formation. *Geochim. Cosmochim. Acta* **70**, 2104–2126.
- Wasson J. W. and Kallemeyn G. W. (1988) Compositions of chondrites. *Philos. Trans. R. Soc. Lond. A* **325**(No. 1587), 535–544.
- Wichman R. W. and Schultz P. H. (1995) Floor-fractured craters in Mare Smythii and west of Oceanus Procellarum: implications of crater modification by viscous relaxation and igneous intrusion models. *J. Geophys. Res.* **100**(E10), 21,201–21,218.
- Wickham S. M. (1987) The segregation and emplacement of granitic magmas. *J. Geol. Soc. Lond.* **144**, 281–297.
- Wilson L. and Keil K. (1991) Consequences of explosive eruptions on small solar system bodies: the case of the missing basalts on the aubrite parent body. *Earth Planet. Sci. Lett.* **104**, 505–512.
- Wilson L. and Keil K. (1996) Clast sizes of ejecta from explosive eruptions on asteroids: implications for the fate of the basaltic products of differentiation. *Earth Planet. Sci. Lett.* **140**, 191–200.
- Wilson L., Keil K., Browning L. B., Krot A. N. and Bourcier W. (1999) Early aqueous alteration, disruption and re-processing of asteroids. *Meteorit. Planet. Sci.* **34**, 541–557.
- Young E. D. (2001) The hydrology of carbonaceous chondrite parent bodies and the evolution of planet progenitors. *Phil. Trans. R. Soc. Lond. A* **359**, 2095–2110.
- Young E. D., Ash R. D., England P. and Rumble D. (1999) Fluid flow in chondritic parent bodies: deciphering the compositions of planetesimals. *Science* **286**, 1331–1335.